

VERY LOW-LUMINOSITY GALAXIES IN THE EARLY UNIVERSE HAVE OBSERVED SIZES SIMILAR TO SINGLE STAR CLUSTER COMPLEXES

R.J. BOUWENS¹, G.D. ILLINGWORTH³, P.A. OESCH⁴, M. MASEDA¹, B. RIBEIRO^{1,5}, M. STEFANON^{1,2}, D. LAM¹
Draft version August 29, 2018

ABSTRACT

We compare the sizes and luminosities of 307 faint $z = 6-8$ sources revealed by the Hubble Frontier Fields (HFF) program with sources in the nearby universe. Making use of the latest lensing models and data from the first four HFF clusters with an extensive suite of public lens models, we measure both the sizes and luminosities for 153 $z \sim 6$, 101 $z \sim 7$, and 53 $z \sim 8$ galaxies. The sizes range over more than a decade from ~ 500 to < 50 pc. Extremely small sizes are inferred for many of our lowest luminosity sources, reaching individual sizes as small as 10-30 pc (the smallest is 11_{-6}^{+28} pc). The uncertainty in these measures ranges from 80 pc for the largest sources to typically about 20 pc for the smallest. Such sizes are smaller than extrapolations of the size-luminosity relation, and expectations for the completeness of our faint samples, suggesting a likely break in the size-luminosity relation at ~ -17 mag with $r \propto L^{0.50 \pm 0.10}$. The sizes and luminosities of the lowest-luminosity sources are similar to those of single star cluster complexes like 30 Doradus in the lower-redshift universe and – in a few cases – super star clusters. Remarkably, our identification of these compact, faint star-forming sources in the $z \sim 6-8$ universe also allow us to set upper limits on the proto-globular cluster LF at $z \sim 6$. Comparisons with recent models allow us to rule out (with some caveats) some scenarios for proto-globular cluster formation and set useful upper limits on other less extreme ones. Our results suggest we may be very close to discovering a bona-fide population of forming globular clusters at high redshift.

1. INTRODUCTION

There are a wide variety of evolved stellar systems in the nearby universe (Norris et al. 2014), from globular clusters (Brodie & Strader 2006; Kruijssen 2014; Renzini et al. 2015) to compact elliptical galaxies (e.g., Faber 1973) to ultra-faint dwarfs (e.g., Simon & Geha 2007) to ultra-diffuse spheroids (e.g., van Dokkum et al. 2015), each of which presumably has its own characteristic formation pathway. The high stellar densities in many of these systems in combination with their old ages (e.g., Forbes & Bridges 2010) suggest that the majority of their star formation occurred at $z \gtrsim 1.5$ when the gas densities in the universe were in general much higher.

One potentially promising way forward to investigate the formation of these local systems is by obtaining a sensitive, high-resolution view into the distant universe. Fortunately, such observations can be obtained by combining the power of long exposures with the Hubble Space Telescope with the magnifying effect of gravitational lensing, as recently implemented in the ambitious Hubble Frontier Fields (HFF) program (Coe et al. 2015; Lotz et al. 2017). Indeed the HFF program has great potential to examine the structure and morphology of faint high-redshift galaxies in great detail. Sources can be stretched by factors of 5 to 20 along one of their axes, allowing the structure in such systems to be studied at

very high spatial resolution. One significant earlier example of what could be done was the highly-magnified $z = 4.92$ galaxy behind MS1358+62 (Franx et al. 1997; Swinbank et al. 2009) where star-forming clumps just 200 pc in size could be partially resolved.

Already there have been several uses of the HFF observations to look in detail at the size distribution of extremely faint galaxies. In an early study leveraging HFF observations over the first HFF cluster Abell 2744, Kawamata et al. (2015) made use of the data to map out the distribution of galaxy sizes vs. luminosities, while Laporte et al. (2016) looked further into the sizes of fainter galaxies using the HFF data over the second and third HFF clusters. Interestingly enough, Kawamata et al. (2015) identified a few ~ -17 mag sources⁶ with nominal physical sizes less than 40 pc using their own lensing model (Ishigaki et al. 2015).

In Bouwens et al. (2017a), we pursued constraints on the physical sizes of fainter > -16.5 mag $z = 2-8$ galaxies in the HFF observations, looking at both (1) the prevalence of sources as a function of lensing shear and (2) detailed size constraints on sources in particularly high magnification areas. These analyses provided the first evidence that very low luminosity (> -16.5 mag) galaxies might have especially small sizes, i.e., in the range of tens of parsecs to over 100 pc. This is very similar to the sizes of molecular clouds and star cluster complexes in the $z \sim 0-3$ universe (e.g., Kennicutt et al. 2003; Bastian et al. 2006; Jones et al. 2010; Swinbank et al. 2012; Adamo et al. 2013; Johnson et al. 2017; Dessauges-Zavadsky et al. 2017).

Finally, Vanzella et al. (2017a) made use of the HFF

⁶ Specifically HFF1C-i10 and HFF1C-i13 from Kawamata et al. (2015).

¹ Leiden Observatory, Leiden University, NL-2300 RA Leiden, Netherlands

² Department of Astronomy, Yale University, New Haven, CT 06520

³ UCO/Lick Observatory, University of California, Santa Cruz, CA 95064

⁴ Observatoire de Genève, 1290 Versoix, Switzerland

⁵ Aix Marseille Univ, CNRS, LAM, Laboratoire d'Astrophysique de Marseille, Marseille, France

observations and their own lensing magnification models (Caminha et al. 2016) to identify a set of very small sources in the $z \sim 3-6$ universe, which Vanzella et al. (2017a) speculated could correspond to proto-globular clusters. To support such a characterization, Vanzella et al. (2017a) made use of the available MUSE spectroscopy on the sources, noting small probable dynamical masses (due to the small measured velocity dispersions) and probable physical associations with brighter neighbors (due to their similar redshifts). In a follow-up analysis, Vanzella et al. (2017b) identified two candidate super star clusters at $z = 3.222$ with sizes of 30 ± 11 pc they inferred to be associated with a brighter neighboring galaxy.

The purpose of the present work is to take one step beyond these studies, using large samples of $z = 6-8$ galaxies to map out the size distribution to very low luminosities,⁷ and exploring the connection with stellar systems at lower redshifts. In doing so, we make use of the first four clusters from the HFF program which have the most refined set of gravitational lensing models, select $z = 6-8$ galaxies behind them, and then measure sizes for individual lensed galaxies. Throughout the paper, we assume a standard “concordance” cosmology with $H_0 = 70$ km s⁻¹ Mpc⁻¹, $\Omega_m = 0.3$ and $\Omega_\Lambda = 0.7$, which is in good agreement with recent cosmological constraints (Planck Collaboration et al. 2015). Magnitudes are in the AB system (Oke & Gunn 1983).

2. DATA SETS AND SAMPLES

In our analysis, we make use of the v1.0 reductions of the HST observations over the first four clusters that make up the Hubble Frontier Fields program (Coe et al. 2015; Lotz et al. 2017). These reductions include all 140 orbits of HST imaging observations obtained over each cluster (70 optical/ACS, 70 near-IR/WFC3/IR) plus any additional archival observations taken over each cluster as a result of other programs, e.g., CLASH (Postman et al. 2012) or GLASS (Schmidt et al. 2014). We focus on results from the first four clusters because version 3 and version 4 public magnification models are already available for those clusters, including multiple image systems identified using the full HFF data set and substantial spectroscopic redshift constraints on multiple image systems (Mahler et al. 2017; Caminha et al. 2017; Schmidt et al. 2014; Vanzella et al. 2014; Limousin et al. 2016; Jauzac et al. 2016; Owers et al. 2011).

Before constructing catalogs of sources behind these clusters, the subtraction of intracluster light and light from the brightest galaxy was performed using GALFIT (Peng et al. 2002) and a median-smoothing algorithm, which will be described in detail in R.J. Bouwens et al. (2017, in prep). As discussed in Appendix A of Bouwens et al. (2017b), our procedure works at least as well as similar procedures in Merlin et al. (2016) and Livermore et al. (2017).

After modeling and subtracting light from the foreground cluster and galaxies from the images, we move onto the selection of faint high-redshift sources. Here we restrict our focus to the selection of sources at $z \sim 6$, $z \sim 7$, and $z \sim 8$ because of the large number of sources in those samples and because they can be selected more

securely than sources at lower redshifts. Some further testing we have performed on the faintest sources (i.e., $H_{160,AB} > 28$) in $z \sim 5$ selections over the HFFs suggest they can be subject to modest contamination from foreground cluster galaxies near the cluster centers. This could be worrisome, since that is where the model magnification factors are frequently high.

The selection of sources in our $z \sim 6$, $z \sim 7$, and $z \sim 8$ samples will be described in R.J. Bouwens et al. (2017, in prep) and rely on the use of two color criteria and optical non-detection criteria, as well as the integrated high and low redshift probability computed with the photometric redshift code EAZY (Brammer et al. 2008). Our procedure for selecting $z \sim 6$ galaxies is almost identical to that already described in Bouwens et al. (2017b), while our procedure for selecting $z \sim 7$ and $z \sim 8$ galaxies is similar to that described in Bouwens et al. (2015). Our $z \sim 6$, $z \sim 7$, and $z \sim 8$ samples from the first four HFF clusters contain 153, 101, and 53 sources, respectively, for a total of 307.

3. REFERENCE SIZE-LUMINOSITY RELATIONS

To provide context for the measurements we obtain of the size and luminosities of faint $z = 6-8$ in the HFF observations (§4), we first provide a brief summary of the general size constraints that exist for galaxies from field studies (§3.1) while reviewing the size measurements that have been made for star cluster complexes in the redshift range $z \sim 0-3$ (§3.2) and star clusters at $z \sim 0$ (§3.3).

3.1. Size-Luminosity Relation for Star Forming Galaxies at $z \sim 6-8$ from Blank Field Studies

It is useful for us to frame the constraints we obtain here for lensed sources in our fields relative to the sizes of galaxies identified in an extensive set of blank field studies (e.g., Ferguson et al. 2004; Bouwens et al. 2004; Oesch et al. 2010; Grazian et al. 2012; Huang et al. 2013; Ono et al. 2013; Shibuya et al. 2015; Holwerda et al. 2015).

The most recent and comprehensive of these determinations is by Shibuya et al. (2015), who conduct size measurements on $\sim 190,000$ $z = 0-10$ galaxies identified over the HUDF, the HUDF parallel fields, the 5 CANDELS fields, and two of the HFF parallel fields. The median half-light radius of sources that Shibuya et al. (2015) measure for their $z \sim 6$ and $z \sim 7$ samples is presented in the left panel of Figure 1 with blue and green circles, respectively, and is well represented by the following relationship:

$$\log_{10}(r_e/\text{pc}) = (-0.4)(0.25)(M_{UV} + 21) + 2.74 \quad (1)$$

where r_e is the half-light radius in pc and M_{UV} is the UV luminosity at $\sim 1600\text{\AA}$. The above size-luminosity is included in Figure 1 as a solid black line over the range where current observations provide a direct constraint on the relationship and extrapolated to lower luminosities assuming the same slope (*dotted line*).

The Shibuya et al. (2015) size-luminosity relation is fairly typical that seen in other studies (Mosleh et al. 2012; Huang et al. 2013; van der Wel et al. 2014) for luminous galaxies across a range of redshifts, from $z \sim 2$ to $z \sim 6$.

It is valuable to recognize that current blank-field observations only probe the high end of the luminosity

⁷ See also new work by Kawamata et al. (2017).

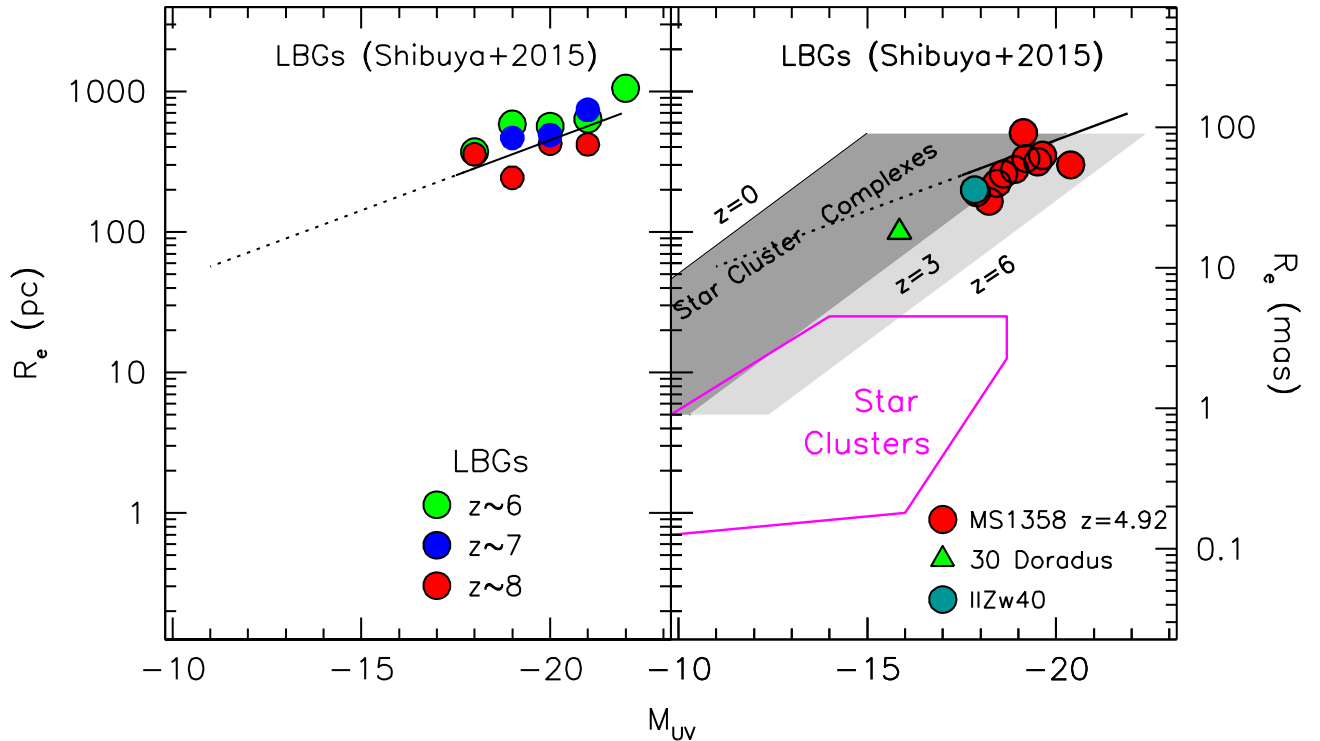


FIG. 1.— Median size vs. luminosity relation of galaxies identified in blank field studies, i.e., the HUDF and CANDELS (*left panel*) and those of star cluster complexes (*right panel*). The canonical size-luminosity relation is presented using both the Shibuya et al. (2015) fit results (*black line*) and median sizes at $z \sim 6$ (*green circles*), $z \sim 7$ (*blue circles*), and $z \sim 8$ (*red circles*). The black dotted line shows an extrapolation of the best-fit Shibuya et al. (2015) trend to lower luminosities. The dark gray region indicates the size-luminosity relation for star cluster complexes in $z = 0-3$ galaxies inferred by Livermore et al. (2015) by fitting to the $z = 0$ results from SINGS (Kennicutt et al. 2003), as well as the results of Jones et al. (2010), Swinbank et al. (2012), Livermore et al. (2012), Wisnioski et al. (2012), and Livermore et al. (2015). The light gray region indicates the size-luminosity relation for star cluster complexes extrapolating this relation to $z = 3-6$. The solid red circles correspond to the measured sizes and equivalent UV luminosities of the star cluster complexes identified in the highly magnified $z = 4.92$ galaxy behind MS1358+62 (Franx et al. 1997) by Swinbank et al. (2009) and Jones et al. (2010), while the solid green triangle and cyan circle correspond to the sizes and luminosities of 30 Doradus and IIZw40, respectively (English & Freeman 2003; Vanzani et al. 2008). The magenta lines enclose the luminosities and sizes measured for star clusters and super star clusters at $z \sim 0$ (Meurer et al. 1995).

range examined in this study.

3.2. Size-Luminosity Relations for Star Cluster Complexes at $z < 3$

A second valuable reference point for the size measurements we will make for faint $z = 6-8$ sources in the HFF observations are star cluster complexes commonly located within star-forming galaxies at $z = 0$ (Kennicutt et al. 2003; Bastian et al. 2005) and which can be seen out to $z \sim 3$ in strongly lensed galaxies (Jones et al. 2010; Wisnioski et al. 2012; Livermore et al. 2012, 2015; Swinbank et al. 2012; Adamo et al. 2013; Vanzella et al. 2017b; Dessauges-Zavadsky et al. 2017).

Star cluster complexes – often referred to as cluster complexes in nearby galaxies – are known to show a range of surface brightnesses at all redshifts where they are observed, i.e., $z \sim 0-3$ (Bastian et al. 2005, 2006; Jones et al. 2010; Swinbank et al. 2012; Wisnioski et al. 2012; Rodríguez-Zaurín et al. 2011; Kennicutt et al. 2003). Star cluster complexes are also described as star-forming clumps (or giant HII regions) when observed in distant galaxies. A simple fit to the mean surface brightness of star cluster complexes as function of redshift yields the

following relation (Livermore et al. 2015):

$$\log\left(\frac{\Sigma_{clump}}{M_{\odot} \text{ yr}^{-1} \text{ kpc}^{-2}}\right) = (3.5 \pm 0.5) \log(1+z) - (1.7 \pm 0.2) \quad (2)$$

While many other observations of star cluster complexes at intermediate to high redshifts are also consistent with the above trend (Franx et al. 1997; Swinbank et al. 2009; Wuyts et al. 2014; Johnson et al. 2017), some star cluster complexes at $z \sim 0$ have been reported to show much higher (by factors of ~ 100) surface densities of star formation (Fisher et al. 2017).

The implied evolution in the surface brightness of star cluster complexes is essentially identical to what one would infer from dimensional arguments. The sizes of collapsed sources is generally found to scale as $(1+z)^{-1}$ (e.g., Bouwens et al. 2004; Oesch et al. 2010; Ono et al. 2013; Holwerda et al. 2015; Shibuya et al. 2015) and the evolution in dynamical time goes as $(1+z)^{-1.5}$, such that $\Sigma_{SFR} \propto r^{-2} t_{dyn}^{-1} \propto (1+z)^{3.5}$. Nevertheless, it should be recognized that the best-fit evolution in Σ_{clump} with redshift likely suffers from surface brightness selection effects (as only the highest surface brightness star cluster complexes can be identified at a given redshift), so the evolution suggested by Eq. 2 should only be considered indicative.

We include a gray-shaded trapezoid in Figure 1 to show the region in size-luminosity parameter space star cluster complexes in $z \sim 0$ -3 galaxies have been found to inhabit. The light gray region shows an extrapolation of this relation to $z = 3$ -6. The solid red circles correspond to the measured sizes and equivalent UV luminosities of the star cluster complexes identified in the highly magnified $z = 4.92$ galaxy behind MS1358+62 (Franx et al. 1997) by Swinbank et al. (2009) and Jones et al. (2010), while the solid cyan circle and green triangle correspond to the sizes and luminosities of IIZw40 and 30 Doradus, respectively (English & Freeman 2003; Vanzi et al. 2008).

Even though we present star cluster complexes at a given redshift as having a fixed surface brightness, Wisnioski et al. (2012) have found their size r to vary as $L^{1/(2.72 \pm 0.04)} \sim L^{0.37 \pm 0.01}$ where L correspond to the $H\alpha$ luminosities, such that the most luminous star cluster complexes also had the highest surface brightnesses.

3.3. Size-Luminosity Relation for Star Clusters and Super Star Clusters

Finally, as a third reference point, we consider the region in parameter space occupied by star clusters and super star clusters. Not attempt here will be done to summarize the substantial work has been done on this topic (e.g., Meurer et al. 1995; Rejkuba et al. 2007; Murray 2009; Bastian et al. 2013), but only to indicate where star clusters lie in parameter space.

Meurer et al. (1995) provide a convenient summary of where star clusters lie in terms of their effective radii and UV luminosities M_{UV} in their Figure 14. The purple line in the right panel of Figure 1 demarcates the approximate region in parameter space that star clusters and super star clusters populate. UV luminosities of the star clusters extend from -9 mag to -19 mag, masses range from 10^4 to $10^8 M_\odot$ (Maraston et al. 2004; Cabrera-Ziri et al. 2014, 2016), while the typical effective radii of star clusters range from 0.5 pc to 4 pc (e.g., Lada & Lada 2003).

The most massive ($>10^5 M_\odot$) star clusters are often called super star clusters, with the effective radii extend up to ~ 20 pc (e.g., Meurer et al. 1995; Rejkuba et al. 2007; Murray 2009; Bastian et al. 2013). Meurer et al. (1995) classify any star clusters with UV luminosities greater than -14 mag as super star clusters.

4. SIZES OF $Z \geq 6$ HFF SOURCES

4.1. Measurement Procedure

In fitting the two-dimensional spatial profile of galaxies behind the HFF clusters to measure sizes, we must account for the substantial impact that gravitational lensing from the foreground cluster has on the spatial profile of galaxies.

The relevant quantities in computing the size of a lensed source is both the total magnification factor μ and the source shear. In Bouwens et al. (2017a), we introduced a quantity that we called the shear factor S which we defined as follows:

$$S = \begin{cases} \frac{1-\kappa-\gamma}{1-\kappa+\gamma}, & \text{for } \frac{1-\kappa-\gamma}{1-\kappa+\gamma} \geq 1 \\ \frac{1-\kappa+\gamma}{1-\kappa-\gamma}, & \text{for } \frac{1-\kappa-\gamma}{1-\kappa+\gamma} < 1 \end{cases} \quad (3)$$

where κ is the convergence and γ is the shear. The shear

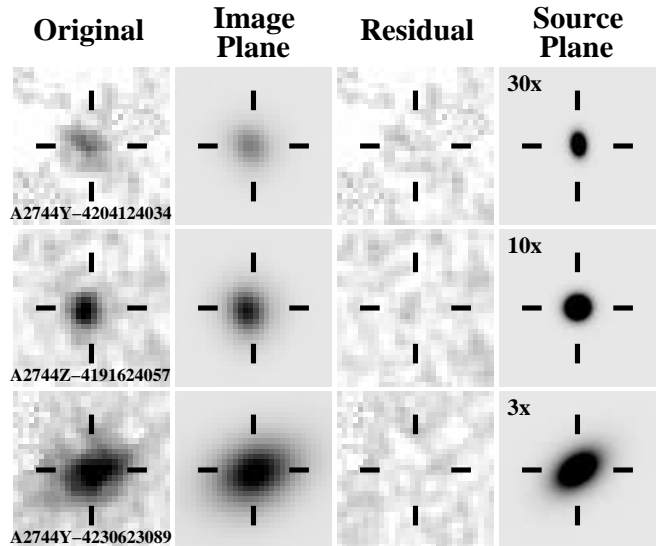


FIG. 2.— Illustration of the typical profile fits used here (§3.1) in deriving half-light radii for sources lensed by the HFF clusters. The source-plane model profiles in the rightmost column (shown at the various zoom factors indicated in the rightmost postage stamp) are transformed into the image plane and convolved with the PSF to produce the model profiles in the image plane (shown in the second leftmost column) for comparison with the observed two-dimensional profile (leftmost column), which is an inverse-weighted mean coaddition of the Y_{105} , J_{125} , JH_{140} , and H_{160} images. The residuals of our profile fits are shown in the second rightmost column.

factor S gives the axis ratio a circular galaxy would have due to the impact of gravitational lensing.

The source magnification μ can be computed from the convergence κ and shear γ maps:

$$\mu = \frac{1}{(1-\kappa)^2 - \gamma^2}$$

The impact of the gravitational lensing on background galaxies is to stretch sources by the factor $\mu^{1/2}S^{1/2}$ along the major shear axis and by the factor $\mu^{1/2}S^{-1/2}$ perpendicular to the major shear axis.

We estimate the half-light radii of sources via a Markov chain Monte-Carlo (MCMC) algorithm where we compare the observed two-dimensional profile with a lensed model profile of a model source with a Sersic radial profile with major and minor axes oriented at some position angle on the sky. In fitting to the two dimensional profile, we coadd the Y_{105} , J_{125} , JH_{140} , and H_{160} images together after scaling to the fluxes in the images to a fixed f_ν frequency and weighting the images by the inverse variance. We coadd the Y_{105} , J_{125} , JH_{140} , and H_{160} PSFs in the same way to derive a composite PSF for the fit procedure. We fix the Sersic parameter to 1, but find similar results (albeit slightly larger sizes by a factor of 1.5) using other Sersic parameters ($n = 2, 3$). Lensing is modeled as magnifying the source by the factor $\mu^{1/2}S^{1/2}$ along the major shear axis and by the factor $\mu^{1/2}S^{-1/2}$ along the minor shear axis.

Figure 2 illustrates our two-dimensional profile fits for three sources in our catalogs, showing the original images (leftmost column), the PSF-convolved model images in the image plane (second leftmost column), the residual image (second rightmost column), and finally the zoomed

TABLE 1
PARAMETRIC LENSING MODELS UTILIZED (SEE ALSO §4.1)^a

Cluster	Model	Version
Abell 2744	CATS	v4.1
	Sharon/Johnson	v4
	Keeton	v4
	GLAFIC	v3
MACS0416	Zitrin/NFW	v3
	CATS	v4.1
	Sharon/Johnson	v4
	Keeton	v4
MACS0717	GLAFIC	v3
	Zitrin/NFW	v3
	Caminha	v4
	CATS	v4.1
MACS1149	Sharon/Johnson	v4
	Keeton	v4
	GLAFIC	v3

^a We only make use of medians of post-HFF parametric lensing models to represent the lensing magnification of sources behind the HFF clusters. Even so, we emphasize that the non-parametric lensing models (GRALE: Liesenborgs et al. 2006; Sebesta et al. 2016, Bradač: Bradač et al. 2009; Hoag et al. 2017, Zitrin-LTM: Zitrin et al. 2012, 2015, Diego: Lam et al. 2014; Diego et al. 2015a, 2015b, 2016a, 2016b, 2017) also perform very well.

model images in the source plane before PSF convolution (*rightmost column*).

We now describe the magnification factors μ and shear factors S that we utilize in our analysis. For the sake of robustness, we do not rely on the results from a single lensing model – since lensing models lack predictive power when the magnification factors from the models become particularly high, as we illustrate for the linear magnification factor $\mu^{1/2}S^{1/2}$ in Appendix A and previously demonstrated in Bouwens et al. (2017b) for the magnification factor. One can do better using the median model (Bouwens et al. 2017b; Livermore et al. 2017).

We therefore take the median magnification and shear factors from all available parametric lens models, including CATS (Jullo & Kneib 2009; Richard et al. 2014; Jauzac et al. 2015a,b; Limousin et al. 2016; Mahler et al. 2017; Lagattuta et al. 2017), Sharon/Johnson (Johnson et al. 2014), GLAFIC (Oguri 2010; Ishigaki et al. 2015; Kawamata et al. 2016), Zitrin-NFW (Zitrin et al. 2013, 2015), Keeton (Keeton 2010), and Caminha et al. (2016, 2017). Each of the four clusters we utilize have highly-refined models available for most but typically not all varieties of model. Our Abell 2744 median model makes use of 5 of the models (v4.1 of CATS, v4 of Sharon/Johnson, v3 of GLAFIC, v3 of Zitrin-NFW, v4 of Keeton), our MACS0416 median model makes use of 6 of the models (v4.1 of CATS, v4 of Sharon/Johnson, v3 of GLAFIC, v3 of Zitrin-NFW, v4 of Keeton, v4 of Caminha), while our MACS0717 and MACS1149 median models make use of 4 of the models (v4.1 of CATS, v4 of Sharon/Johnson, v3 of GLAFIC, v4 of Keeton). Table 1 provides a convenient summary of the models we use.

In general, the parametric lens models appear to perform slightly better in terms of their predictive power

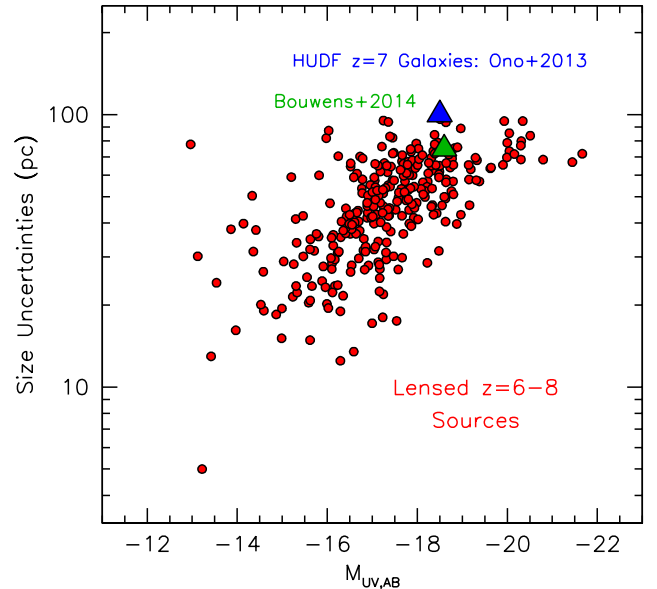


FIG. 3.— Nominal 1σ accuracy with which source sizes can be measured for individually lensed $z = 6-8$ sources identified behind various HFF clusters vs. the UV luminosity inferred (*black crosses*). The accuracy of size measurements is computed by adding in quadrature the size uncertainty based on the MCMC fit results and the size uncertainty resulting from the unknown lensing magnification (based on the dispersion in the lensing models). For comparison, we also show the accuracy with which size measurements were claimed for individual $z = 7-8$ sources from the HUDF data (Ono et al. 2013). Bouwens et al. (2014) estimated a 1σ accuracy of 75 pc based on their analysis of sizes in a stacked $z \sim 7$ source from the HUDF.

than the non-parametric models (Meneghetti et al. 2017) though the non-parametric models (GRALE: Liesenborgs et al. 2006; Sebesta et al. 2016, Bradač: Bradač et al. 2009; Hoag et al. 2017, Zitrin-LTM: Zitrin et al. 2012, 2015, Diego: Lam et al. 2014; Diego et al. 2015a, 2015b, 2016a, 2016b, 2017) also do very well.

In computing the magnification and shear factors for the individual models (to produce the median), we multiply the relevant κ and γ 's from the aforementioned public models by the ratio of the distance moduli D_{ls}/D_s , where D_{ls} is the angular diameter distance between the lensing cluster and source and the angular diameter distance to the source, using the best-fit photometric redshift for the source to compute the distance.

In this way, we compute the median linear magnification factor $\mu^{1/2}S^{1/2}$ and $\mu^{1/2}S^{-1/2}$ along the major and minor shear axes, respectively. It is worth remarking that these linear magnification factors appear to be reliable to values as high as 20, if we take the results of Appendix A as indicative, but not in excess of 20. The direction of the major shear axis is derived using the version 4.1 CATS magnification model, but is fairly similar for the other parametric lensing models.

It is interesting to ask how well we can use the HFF lensing clusters to determine the scale length of faint galaxies to very small sizes. We can look to some recent work from HST imaging observations over the Hubble Ultra Deep Field (Beckwith et al. 2006; Bouwens et al. 2011; Ellis et al. 2013; Illingworth et al. 2013) to provide some indication. Ono et al. (2013) measure source sizes for $z \sim 7-8$ galaxies at ~ -19 mag to a 1σ uncertainty of ~ 100 pc and at ~ -18 mag to a 1σ uncertainty of

TABLE 2
CATALOG OF TINY STAR-FORMING SOURCES^a AT $z \sim 6-8$

ID	R.A.	Decl	M_{UV}	μ^b	μ_{1D}^c	r_e (pc) ^d
A2744I-4205324088 ^{*e}	00:14:20.54	-30:24:08.9	-14.6 ^{+0.6} _{-0.6}	21.5 ^{+15.3} _{-8.8}	6.2 ^{+1.9} _{-2.5}	17 ⁺²⁸ ₋₁₃
A2744I-4222023578	00:14:22.21	-30:23:57.9	-15.6 ^{+0.7} _{-1.2}	50.1 ^{+41.4} _{-33.6}	8.5 ^{+4.4} _{-3.8}	31 ⁺³² ₋₁₃
A2744I-4212723104	00:14:21.28	-30:23:10.5	-16.0 ^{+0.1} _{-0.1}	6.4 ^{+0.5} _{-0.8}	5.7 ^{+0.4} _{-1.2}	32 ⁺²⁴ ₋₁₇
A2744Y-4204124034 [*]	00:14:20.41	-30:24:03.5	-14.0 ^{+1.2} _{-1.6}	75.0 ^{+151.2} _{-58.0}	15.1 ^{+24.0} _{-9.5}	14 ⁺²⁹ ₋₉
M0416I-6055105026	04:16:05.52	-24:05:02.7	-14.6 ^{+0.4} _{-0.4}	18.0 ^{+47.0} _{-6.1}	16.3 ^{+35.8} _{-6.1}	40 ⁺²⁶ ₋₂₇
M0416I-6090604399	04:16:09.06	-24:04:40.0	-15.3 ^{+0.3} _{-0.5}	11.6 ^{+3.4} _{-4.6}	7.3 ^{+2.4} _{-3.4}	32 ⁺³⁸ ₋₁₃
M0416I-6095704260 [*]	04:16:09.57	-24:04:26.1	-15.0 ^{+0.3} _{-0.2}	12.5 ^{+3.3} _{-2.5}	8.0 ^{+2.5} _{-2.0}	28 ⁺¹⁹ ₋₁₂
M0416I-6120203507	04:16:12.02	-24:03:50.8	-13.6 ^{+1.2} _{-1.4}	62.7 ^{+121.6} _{-45.6}	57.6 ^{+91.5} _{-42.7}	18 ⁺⁵³ ₋₁₁
M0416I-6118103480 ^{*†}	04:16:11.81	-24:03:48.1	-15.0 ^{+1.3} _{-1.0}	33.6 ^{+81.6} _{-19.9}	24.5 ^{+85.1} _{-15.2}	16 ⁺²⁹ ₋₁₃
M0416I-6130803432 [‡]	04:16:13.09	-24:03:43.3	-17.3 ^{+0.2} _{-0.6}	3.5 ^{+0.7} _{-0.6}	3.4 ^{+0.3} _{-0.6}	38 ⁺³⁶ ₋₂₇
M0416I-6115434445 ^{†,‡}	04:16:11.54	-24:03:44.5	-14.5 ^{+0.9} _{-1.0}	43.0 ^{+54.2} _{-25.4}	31.0 ^{+48.0} _{-18.4}	21 ⁺³¹ ₋₁₃
M0416I-6106703335 [*]	04:16:10.67	-24:03:33.6	-16.3 ^{+0.3} _{-0.2}	11.1 ^{+3.7} _{-2.0}	8.8 ^{+3.1} _{-0.7}	33 ⁺¹³ ₋₁₂
M0416I-6114803434 ^{†,‡}	04:16:11.48	-24:03:43.5	-17.0 ^{+0.3} _{-0.5}	21.3 ^{+6.3} _{-7.6}	14.9 ^{+7.8} _{-4.8}	38 ⁺²¹ ₋₁₄
M0416Y-6088104378 [*]	04:16:08.82	-24:04:37.9	-13.4 ^{+1.0} _{-1.1}	62.1 ^{+90.8} _{-39.5}	38.3 ^{+45.7} _{-27.0}	11 ⁺²⁸ ₋₆
M0717I-7354743496	07:17:35.48	37:43:49.7	-13.9 ^{+1.6} _{-1.4}	57.7 ^{+205.4} _{-42.1}	46.8 ^{+127.4} _{-34.3}	27 ⁺⁷² ₋₂₀
M0717I-7374244282	07:17:37.43	37:44:28.3	-15.0 ^{+0.8} _{-0.8}	9.6 ^{+10.8} _{-5.0}	3.6 ^{+1.5} _{-0.9}	34 ⁺³⁸ ₋₂₂
M0717I-7361844009 [*]	07:17:36.18	37:44:01.0	-13.2 ^{+0.3} _{-0.4}	67.2 ^{+18.6} _{-22.1}	22.2 ^{+3.6} _{-1.2}	23 ⁺⁵ ₋₅
M0717I-7357345028	07:17:35.74	37:45:02.9	-14.4 ^{+1.2} _{-1.6}	26.8 ^{+54.2} _{-20.5}	19.0 ^{+58.5} _{-14.5}	24 ⁺⁷⁹ ₋₁₈
M0717Z-7390844017 [‡]	07:17:39.09	37:44:01.8	-17.1 ^{+0.4} _{-1.8}	21.8 ^{+10.7} _{-17.8}	17.7 ^{+14.4} _{-13.3}	24 ⁺⁷⁵ ₋₁₁
M0717Z-7401344384	07:17:40.14	37:44:38.5	-16.1 ^{+0.0} _{-0.7}	8.3 ^{+0.3} _{-2.9}	6.4 ^{+1.5} _{-2.3}	39 ⁺³³ ₋₁₅
M0717Z-7311744437	07:17:31.18	37:44:43.8	-16.0 ^{+0.8} _{-0.4}	8.2 ^{+8.8} _{-2.6}	4.0 ^{+3.1} _{-0.7}	27 ⁺³⁰ ₋₁₈
M0717Y-7336744331	07:17:33.68	37:44:33.2	-14.4 ^{+2.3} _{-1.3}	43.1 ^{+312.6} _{-29.9}	7.6 ^{+40.9} _{-3.7}	31 ⁺³⁸ ₋₂₆
M0717Y-7329744137	07:17:32.97	37:44:13.8	-15.3 ^{+0.9} _{-0.6}	13.7 ^{+16.8} _{-5.9}	7.5 ^{+8.6} _{-3.7}	34 ⁺⁴² ₋₁₉
M1149I-9384023344	11:49:38.40	22:23:34.5	-13.0 ^{+2.6} _{-2.4}	124.7 ^{+1226.2} _{-111.1}	90.7 ^{+949.9} _{-81.8}	26 ⁺²⁵² ₋₂₄
M1149I-9379223320	11:49:37.93	22:23:32.1	-13.1 ^{+0.4} _{-1.2}	74.7 ^{+37.3} _{-49.4}	39.8 ^{+31.6} _{-24.6}	35 ⁺⁵⁷ ₋₁₆
M1149Y-9377423253 [*]	11:49:37.74	22:23:25.4	-14.9 ^{+0.1} _{-0.3}	16.2 ^{+2.0} _{-4.1}	7.9 ^{+1.3} _{-3.9}	19 ⁺³¹ ₋₁₁

^a All sources with inferred half-light radii less than 40 pc are included in this table. Star forming sources could include star cluster complexes, super star clusters, proto-globular clusters, or especially compact galaxies

^b Median magnification factors (and 1σ uncertainties) derived weighting equally the latest public version 3/4 parametric models from each lensing methodology (§4.1).

^c μ_{1D} are the median one-dimensional magnification factors (and 1σ uncertainties) along the major shear axis $\mu^{1/2}S^{1/2}$ weighting equally the parametric models from each lensing methodology. This is the same quantity as μ_{tang} reported by Vanzella et al. (2017a).

^d Inferred half-light radius in physical units. The quoted uncertainties include both uncertainties in the spatial fits and uncertainties in the lensing model.

^e The eight sources where the upper 1σ limit on the inferred half-light radius is less than 50 pc are marked with an “*.”

[†] Tiny star-forming source also presented in Vanzella et al. (2017a).

[‡] Source also has an inferred size of ≤ 40 pc in the Kawamata et al. (2017) catalog.

~ 150 pc, corresponding to ~ 0.1 native pixel length. In Bouwens et al. (2014), the sizes of a stack of $z \sim 7$ galaxies are measured to an estimated 1σ accuracy of 75 pc at ~ -18.5 . If we assume that the median linear magnification factors are accurate to factors of 20, this means we can measure source sizes to $20\times$ higher spatial resolution over the HFF clusters as we can over the Hubble Ultra Deep Field. This means we can potentially measure the linear sizes of sources to a 1σ accuracy of 4-5 pc.

In Figure 3, we provide a sense for the accuracies with which we can measure sizes for our lensed $z = 6-8$ samples vs. UV luminosity. The accuracy of size measurements is computed by adding in quadrature the size uncertainty based on the MCMC fit results and the size uncertainty resulting from the unknown lensing magnification (based on the dispersion in the lensing models). This suggests a typical half-light radius measurement accuracy of 50 pc and 10 pc for sources at -18 mag and -15 mag, respectively.

4.2. Size vs. Luminosity Results

In the upper left panel of Figure 4, we show the measured sizes and estimated luminosities of lensed sources in our $z = 6-8$ samples in relation to the derived and extrapolated size-luminosity relation from blank field studies. We also indicate in this panel where our source recovery experiments from Bouwens et al. (2017a, 2017b) indicate that our selection would be less than 20% complete (*blue dashed line*).

Given uncertainties in our knowledge of the magnification factors for specific lensed sources behind the HFF clusters, we also present in the upper right panel of Figure 4 the source sizes and luminosities, capping the linear magnification factor and magnification factors to values of 20 and 30, respectively. The position of sources in parameter space is similar to the upper left panel, but with fewer sources at especially small sizes and low luminosities.

Interestingly enough, at the bright end (< -17 mag), lensed sources in our samples scatter around extrapolated expected sizes from blank-field studies, with a best-fit trend such that half-light radius scales with luminos-

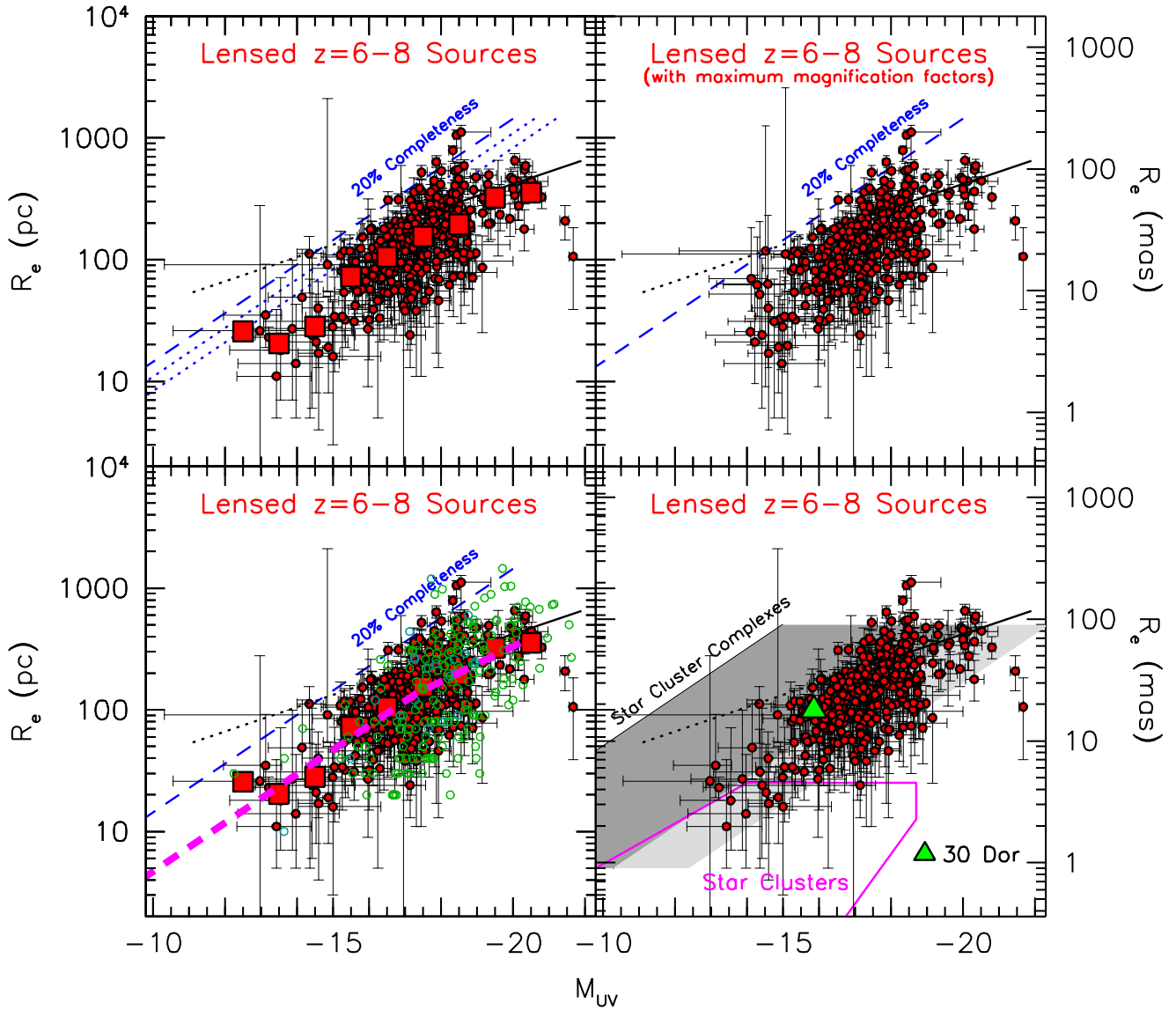


FIG. 4.— Comparison of the distribution of sizes and luminosities for $z = 6-8$ galaxies in the HFFs with a canonical size-luminosity relationship from blank field studies (black solid and dotted line in all panels) and those of star cluster complexes (lower right panel). The canonical size-luminosity relation for galaxies and star cluster complexes is as in Figure 1. For the sizes and luminosities of individual lensed $z = 6-8$ galaxies, the results (red circles and 1σ limits) are based on the median magnification factors from the parametric models (upper left, lower left, and lower right panels) and where we impose a maximum linear magnification factor of 20 (upper right panel) for greater robustness. 1σ errors on the inferred sizes and UV luminosities are quoted based on the 68% confidence intervals in the size fits and the range of magnification factors in the parametric lensing models. The blue dashed line delimits the region where our selections are expected to be less than 20% complete. The blue dotted lines directly to the right of the blue dashed lines delimit the regions where our selections are expected to be 50% and 80% complete relative to the maximum. As these completeness limits crosses the standard size-luminosity relation at ~ -15 mag, we might expect selections in the HFFs to be significantly incomplete at > -15 mag, if this relation applied to the lowest luminosity $z = 6-8$ galaxies. If our selections are largely complete, the dashed magenta line (lower left panel) shows the asymptotic form for the size-luminosity relation (where radius $\propto L^{0.5}$). Similar trends are seen in the size vs. luminosity for lower luminosity ($M_{UV,AB} > -19$) galaxies by Kawamata et al. (2017: light green open circles) and Laporte et al. (2016: light open cyan circles). Faint $z \sim 6-8$ galaxies also exhibit very similar sizes to that seen for star cluster complexes like 30 Doradus at $z \sim 0$ (solid green triangle) and some star cluster complexes at $z \geq 2$ (lower right panel). The magenta lines demarcate the star cluster region as shown in Figure 1.

ity as $L^{0.26 \pm 0.03}$. However, as one considers the size-luminosity relation defined by our sample to lower luminosities, one sees a trend to very small sizes with an asymptotic slope radius $\propto L^{0.50^{+0.10}_{-0.11}}$ where L is luminosity (magenta dashed line):

$$r_e = (72_{-5}^{+6} \text{ pc}) 10^{-0.4(M_{UV}+16)(0.50^{+0.10}_{-0.11})}$$

The measured size-luminosity relation derived by Kawa-

mata et al. (2017: light green open circles) and Laporte et al. (2016: cyan open circles) for lower-luminosity galaxies follows a similar trend. In deriving the radius vs. luminosity relation, the intrinsic scatter found by Shibuya et al. (2015), i.e., 0.2 dex, is added in quadrature to the measurement errors. In Bouwens et al. (2017a) and Kawamata et al. (2017), the reported dependence of size on luminosity are $\propto L^{0.50 \pm 0.07}$ and $\propto L^{0.46^{+0.08}_{-0.09}}$, respec-

tively.

There are reasons for supposing that the observed trend might arise due to surface brightness selection effects, uncertainties in the lensing models, or a combination of the two effects. Indeed, surface brightness selection effects (e.g., Bouwens et al. 2004; Oesch et al. 2015; Taghizadeh-Popp et al. 2015) might cause us to recover a $r \propto L^{0.50^{+0.10}_{-0.11}}$ correlation between size and luminosity, as was pointed out in both Bouwens et al. 2017a and Ma et al. 2017. The dashed line in Figure 4 show the sizes and luminosities where source selection fraction is only 20% efficient (vs. the maximum) using the simulations in Bouwens et al. (2017a, 2017b), while the dotted lines in the upper left panel of Figure 4 show the sizes and luminosities where the selection fraction is 50% and 80%. Such a correlation between source size and luminosity would only be enhanced by uncertainties in the lensing model (scattering sources along the same general radius-luminosity vector).

It is obviously useful to examine the form of the size luminosity relation to very luminosities in a way that are robust against such worries. In principle, such is possible relying on the faintest $z \sim 4$ sources identified over the HUDF. In appendix B, we provide an independent measurement of the median sizes of $z \sim 4$ galaxies as a function of the UV luminosity, and compare the median sizes with what we derive from a faint $z \sim 4$ selection behind the HFF clusters.

Beyond the plausibility tests we provide on our size-luminosity measurements in Appendix C, there are two other arguments we can make which provide some support to our overall constraints on the median measured sizes of galaxies vs. UV luminosity. This first argument (§4.3) relies on the impact the size distribution has on the form of the UV LF at >-15 mag (§4.3) and the second argument (§4.4) relies on simulations designed to estimate the impact of the model uncertainties on the number of small sources recovered in our HFF samples.

Assuming that these arguments are valid (and the results in Appendix C are indicative), our results indicate a break in the size-luminosity relation at $M_{UV} \sim -17$ mag, such that the sizes of galaxies transition from lying along the size-luminosity relation of more luminous galaxies to possessing sizes and luminosities more similar to star cluster complexes in $z = 0-3$ galaxies (Bastian et al. 2006; Jones et al. 2010; Livermore et al. 2012, 2015; Wisnioski et al. 2012; Swinbank et al. 2012; Johnson et al. 2017), as explicitly shown in the lower right panel of Figure 4. In fact, the typical -15 mag galaxy in our samples has a smaller half-light radius than 30 Doradus, which has a measured half-light radius of ~ 100 pc (*lower right panel of Figure 4*).

It has been suggested that some lensed high-redshift sources behind the HFF clusters may in fact be super star clusters (Vanzella et al. 2017a, 2017b; Bouwens et al. 2017a [§6.1]). It is interesting therefore to ask if any sources from our samples seem consistent with corresponding to super star clusters. In Table 2 we provide such a compilation, including all sources with estimated half-light radii that could plausibly correspond to super star clusters. As sizes of super star clusters from 4 pc to 20 pc, we include sources with estimated sizes up to 40 pc.

The uncertainties we report on the measured sizes include a 1σ error computed based on the range in linear magnifications predicted by the parametric lensing models. The uncertainties in the measured sizes for sources in Table 2 are substantial. Only two of the sources have measured sizes less than 40 pc after allowing for the 1σ uncertainties in the measured sizes and from the lensing models. Eight of the sources are within an upper bound of 50 pc (a slightly less stringent limit) allowing for the 1σ uncertainties. These sources are indicated in Table 2 with a “*”.

4.3. Impact of Uncertainties in the Lensing Model

We have only an approximate measure of the lensing magnification from the foreground clusters in the HFF clusters and therefore we could expect uncertainties from the lensing models to impact our derived size vs. luminosity results. In particular, errors in the recovered properties of lensed sources are such as to scatter sources so that their measured half-light radii r would show a steeper relationship vs. luminosity L . For cases where errors in the lensing model impacted either both magnification axes equally or just a single magnification axis, sources would scatter such that $r \propto L^{0.5}$ or $r \propto L$, respectively.

One way of illustrating the impact these uncertainties would have on our results is to create a mock set of sources behind the first four HFF clusters based on the Shibuya et al. (2015) size-luminosity relation, the Bouwens et al. (2017b) $z \sim 6$ UV LF, and an assumed scatter around the size-luminosity relation of 0.22 dex (as Shibuya et al. 2015 find). In creating the mock data set with apparent magnitudes and sizes for individual sources, we will assume the CATS v4.1 lensing models represent the truth and then interpret the results using a median of the other parametric lensing models. This mirrors the forward-modeling approach we previously utilized in Bouwens et al. (2017b) to derive $z \sim 6$ LF results from our catalogs of $z \sim 6$ sources behind the first four HFF clusters.

Figure 5 illustrates the impact of these uncertainties on the size-luminosity relation. The left panel in this figure shows the input distribution of sizes and luminosities, while the right panel shows the recovered distribution after using a median model to interpret the mock data set. The red solid squares show the median half-light radius recovered per 1-mag bin of UV luminosity.

Comparisons of the left and right panels from Figure 5 show the fairly dramatic impact of the lensing model uncertainties on the recovered sizes or luminosities for specific sources. Brightward of -15 mag, the median recovered size in a luminosity bin is very close to that from the input model. However, faintward of -15 mag, the median recovered sizes in a luminosity bin become substantially smaller. This is due to the fact that at lower luminosities, many sources from bright magnitude bins are both scattering into the lower luminosity bins and scattering towards smaller sizes, such that the median sizes are substantially smaller than the input sizes. One can see how brighter sources can contaminate the lowest-luminosity bins inspecting the results from Appendix B – where it is shown that the true median luminosity of sources in the -12.5 -mag, -13.5 -mag, and -14.5 -mag bins are all ~ -15 mag.

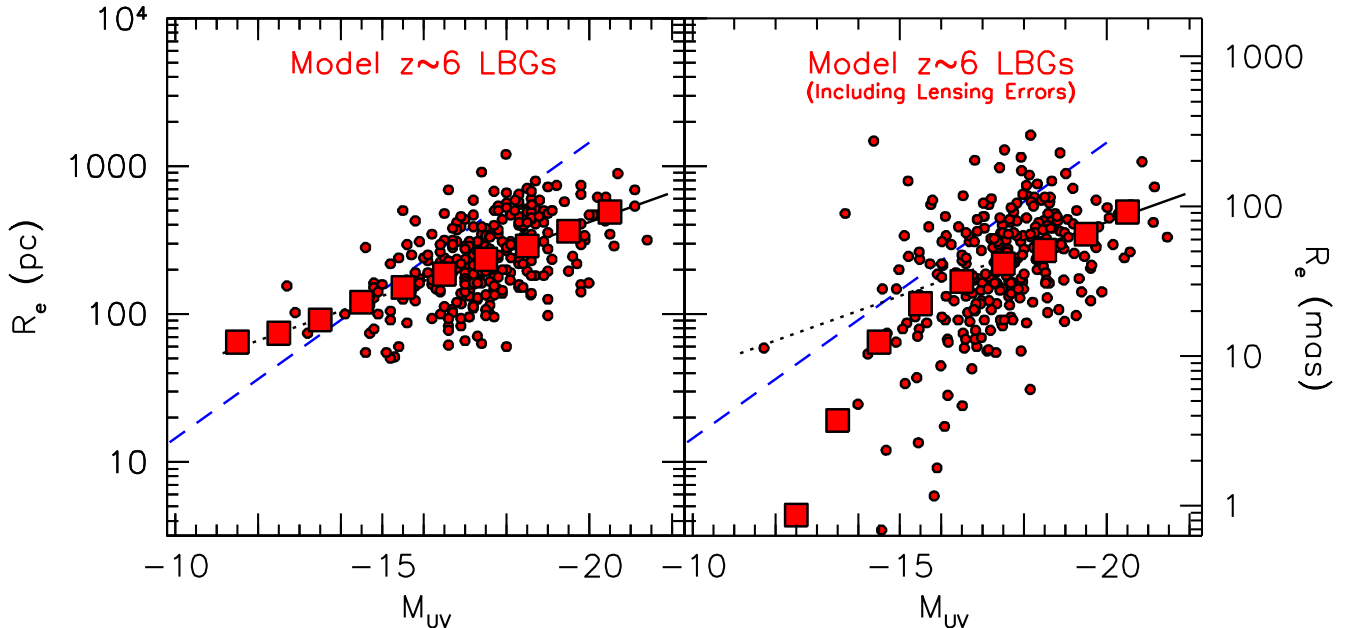


FIG. 5.— Illustration of how errors in the lensing models are expected to impact the size-luminosity distribution using Monte-Carlo simulations. The left panel shows an input distribution of sizes and luminosities for a ~ 300 source sample (shown with the red solid points) using the size-luminosity relation from the Shibuya et al. (2015). The right panel shows the recovered distribution of sizes and luminosities derived treating the CATS models as the truth and using the median magnification and shear maps from the parametric lensing models. The red squares show the median size at a given UV luminosity – with the median shown with the red squares – before and after applying the median magnification and shear maps. The red median sizes are derived based on $100\times$ more sources than are shown on the figure. No selection effects are included in these idealized results. Errors in the lensing models can introduce significant scatter in the recovered sizes and UV luminosities, but do not appreciably impact the recovered median size measurements brightward of -15 mag (but do so at fainter luminosities, see §4.3). Nevertheless, we find a slightly larger number of small <40 -pc sources in the observations, i.e., 26, than in these simulations (typically 15), suggesting that some of the small sources are likely bona-fide.

In addition, the results from Appendix B allow us to assess the impact of errors in the lensing models on the number of extremely small sources. From the input model, only ~ 1 source in an input sample of ~ 300 sources would be expected to have a half-light radius <40 pc. However, after including uncertainties from the lensing models, ~ 15 sources are expected to have such small inferred sizes, indicating that some of the nominally small sources in our sample may be there due to observational scatter. For comparison, there are 26 such sources in our own sample with half-light radii <40 pc. Therefore, our recovered total using the actual observations is larger than the simulated total by 2σ . This suggests that some of the nominally compact sources do indeed have sizes <40 pc, but many may actually be somewhat larger.

The present exercise illustrates the need for caution in making claims about specific small star-forming sources behind lensing clusters.

4.4. Implications from the Faint End Form of the $z \sim 6$ LF Derived from the HFFs

There is a direct connection between (1) the distribution of sizes and surface brightnesses assumed for the lowest luminosity galaxies and (2) the faint-end form inferred for the UV LFs at $z \sim 2-6$ (see Figures 6 and 7). The purpose of this section is to spell out this connection and the impact one has for the other.

4.4.1. Implications of Standard Shallow Size-Luminosity Relations for the Faint-End Form of the UV LFs

As we previously discussed in §3.1 above, blank-field studies have found the median half-light radius of

brighter galaxies depends on the luminosity L of galaxies as $R \propto L^{0.25}$ (Shibuya et al. 2015), across a wide range of redshifts. Huang et al. (2013) find a similar scaling at $z \sim 4$ and $z \sim 5$, and we might expect similar scalings to apply to higher redshift galaxies if we extrapolate the size-mass relations obtained by van der Wel et al. (2014). The well-known Kravtsov (2013) relation between halo mass and galaxy size (their Figure 1) also argues for approximately such a scaling. Finally, both theoretical models (e.g., Liu et al. 2017) and also some high-resolution hydrodynamical simulations, e.g., Ma et al. (2017), report recovering almost exactly this scaling in star-forming galaxies at high redshifts to very low luminosities.

If these scalings apply to extremely low luminosity $z \sim 6-8$ galaxies, the surface brightness should vary as $L/R^2 \propto L^{0.5}$. With such a scaling, $0.001L^*$ (-13.5 mag) galaxies would have surface brightnesses $30\times$ lower than L^* galaxies have. At such low surface brightnesses, we would expect searches for faint $z = 2-8$ galaxies to be highly incomplete. This would translate into significantly lower surface densities of $z \sim 6$ candidates in the highest magnification regions, relative to that seen in lower magnification regions.

Are such a deficit of sources seen in the very high magnification ($\mu > 10$) regions relative to lower magnification ($\mu < 5$) regions? In Bouwens et al. (2017b), we find essentially an identical surface density of $z \sim 6$ sources in both low and high magnification regions. Ishigaki et al. (2017) also find a high surface density of $z \sim 6$ galaxies to ~ 29 mag in their catalogs even in high magnification $\mu > 18$ regions, i.e., their Figure 1.

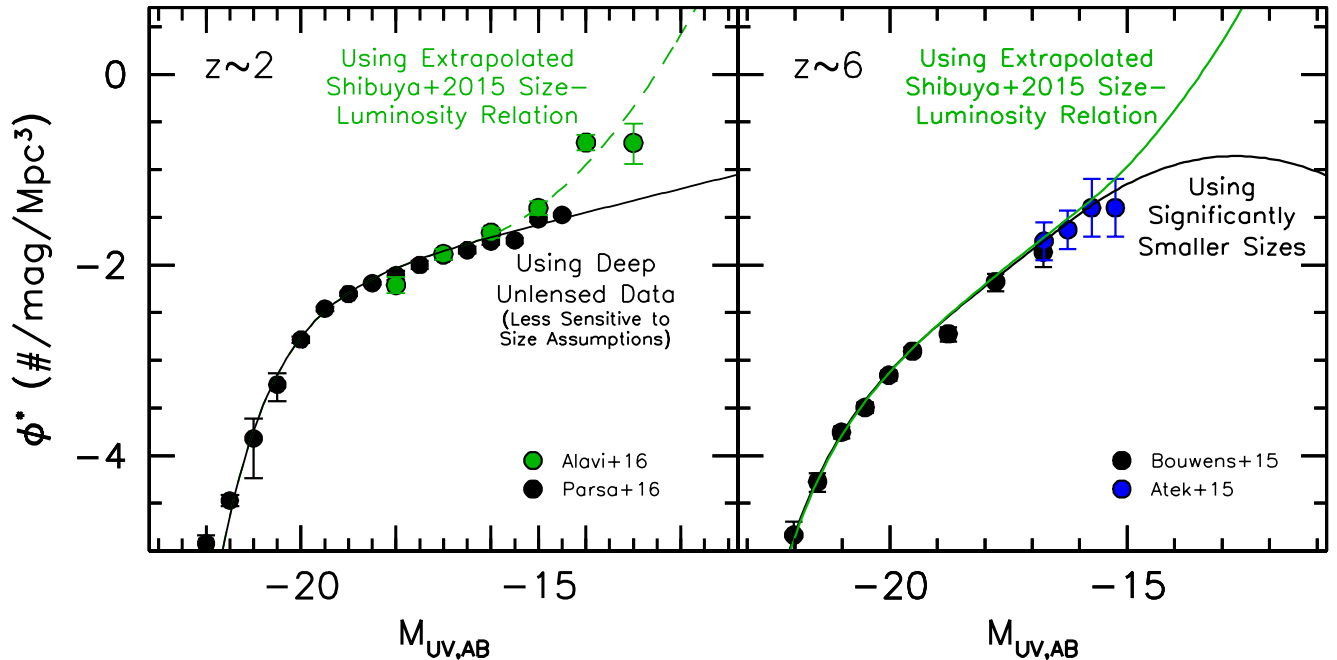


FIG. 6.— An illustration of the significant impact the galaxy size distribution has on the faint-end (>-15 mag) form of the galaxy $z = 2-8$ LFs. Given that the requisite completeness corrections for LF determinations are directly calculable from the assumed size-luminosity relation, presumptions regarding the faint-end form of the LF are directly connected to what supposes the size distribution of faint galaxies to be. If faint $z \sim 2$ and $z \sim 6$ galaxies have sizes which are a simple extrapolation of the Shibuya et al. (2015) size-luminosity relation, the recovered UV LFs at $z \sim 2$ and $z \sim 6$ combining blank field and lensing cluster observations are as indicated by the green lines and points (Alavi et al. 2016; §5.4 of Bouwens et al. 2017b). Meanwhile, if faint galaxies are assumed to have significantly smaller sizes than inferred from an extrapolation of the Shibuya et al. (2015) – or equivalently a break in the size-luminosity relation: see magenta dashed line in the lower left panel of Figure 4 – the recovered UV LFs show much lower volume densities. The black line in the right panel are the Bouwens et al. (2017b) LF results and rely on significantly smaller size assumptions than the extrapolated Shibuya et al. (2015) relation. The right panel also shows the blank field $z \sim 6$ LF results from Bouwens et al. (2015) along with the results of Atek et al. (2015). Meanwhile, the black line in the left panel are from Parsa et al. (2016) derive from the sensitive blank field observations over the HUDF (black line and black circles) where size assumptions are not especially important at the faint end where sources are smaller than the PSF. If we suppose – following most theoretical models – that the UV LF at $z \sim 2$ and $z \sim 6$ extends towards fainter luminosities with a fixed (or progressively flatter) faint end slope, then the size-luminosity relation cannot extend to the lowest luminosity galaxies following the Shibuya et al. (2015) scaling, but must show a break at some luminosity towards a steeper scaling.

If we apply the expected high incompleteness in high magnification regions (from the extrapolated Shibuya et al. 2015 relation) to the Bouwens et al. (2017b) search results, we would infer very high volume densities for the ultra-low luminosity sources at $z \sim 6$. In fact, this would translate into a concave-upwards faint-end form for the UV LF at $z \sim 6$, as was inferred in §5.4 of Bouwens et al. (2017b) also applying the extrapolated Shibuya et al. (2015) size-luminosity relation. This is illustrated with the green solid line in the right panel of Figure 6.

Earlier, applying an extrapolation of the size-luminosity relation obtained by Shibuya et al. (2015) for $z \sim 2$ galaxies – with a similar size-luminosity dependence to their $z \sim 6$ results – Alavi et al. (2016) had derived a UV LF at $z \sim 2$ showing exactly such a concave-upward form. This is indicated with the green solid line in the left panel of Figure 6.

Similar to the large-size analysis provided by the Bouwens et al. (2017b) in their §5.4, Atek et al. (2015) and Castellano et al. (2016) made use of standard shallow size-luminosity relations in deriving LF at $z \sim 6-7$, only obtaining plausible LF results through the restriction of their determinations to sources brightward of -15 mag. H. Atek (private communication) indicated to us that they did not extend their LF results faintward of -15 mag, due to uncertainties in extrapolating the size-

luminosity relation into this regime and the very high volume densities implied at such faint magnitudes by the uncertain incompleteness corrections.

While Atek et al. (2015) did not discuss the prevalence of >15 mag galaxies at $z \sim 6-8$, Livermore et al. (2017) show results down to -12.5 mag. The sizes that Livermore et al. (2017) quote for their faint galaxies correspond to a median size of 0.5 kpc for their faint sample, but as noted previously (Bouwens et al. 2017a,b) incompleteness effects would be extreme for such large sizes. The surface brightness of -12.5 -mag ($0.0004L^*$) sources would be $2500\times$ lower than for L^* sources and result in very high completeness corrections at the low luminosity end. When we carry out a comparable analysis to Livermore et al. (2017) we find that we cannot reproduce their derived luminosity function with such large sizes (see also Kawamata et al. 2017); we can only broadly reproduce their results when we use a smaller size distribution. It is not clear what the reason is for this discrepancy, but we note that the combination of the median size and derived LF in Livermore et al. (2017) do not fit comfortably in the “flow chart” of Figure 7 here.

4.4.2. Possibility of a Steep Size-Luminosity Relation?

While one would expect to derive a “concave-upwards” luminosity function for galaxies at $z \sim 6$ making use of the standard shallow size-luminosity relation for

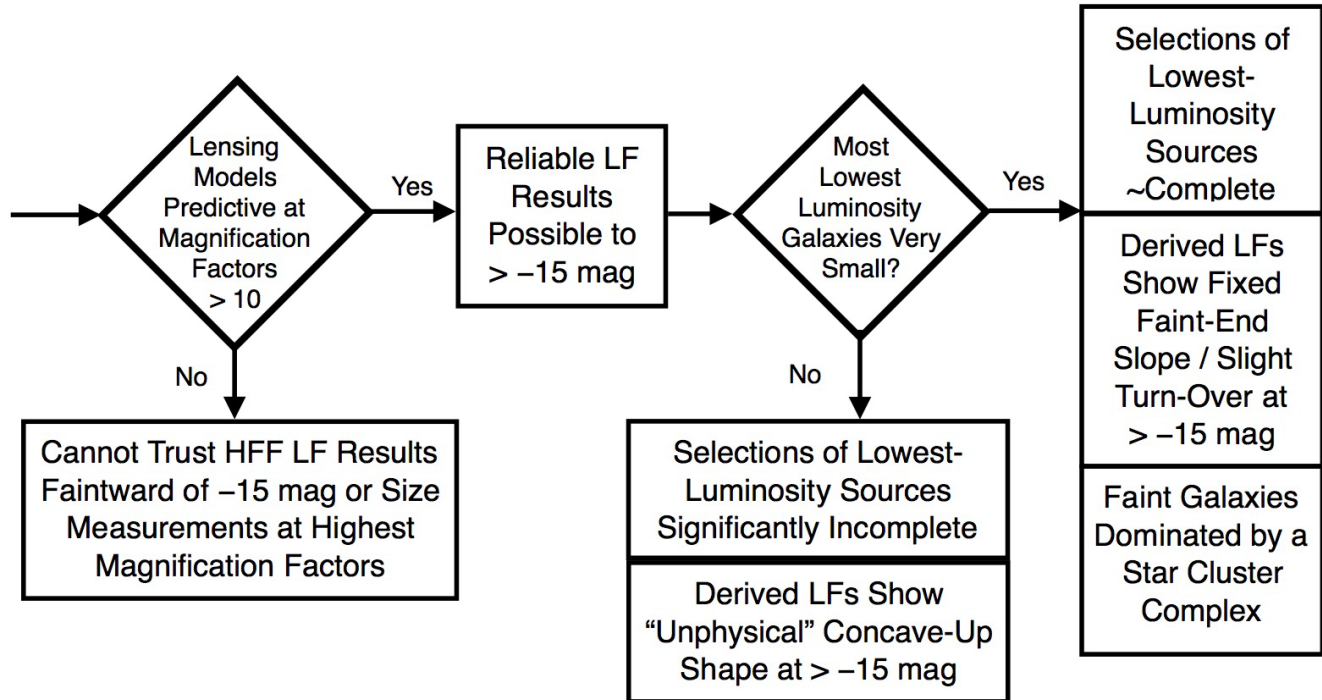


FIG. 7.— A simple flowchart summarizing the connection between the form of the UV LF at high-redshift and the implied size distribution for lower luminosity galaxies (see §4.4). As the various possibilities summarized by this logical flowchart rely on the HFF lensing models being predictive to magnification factors of >10 (e.g., as the Meneghetti et al. 2017; Prieuwe et al. 2017; Bouwens et al. 2017b results suggest), such a condition is included as the first step in the decision tree. If we assume that the lower-luminosity galaxies have sizes that simply follow an extrapolation of the Shibuya et al. (2015) size-luminosity relation (where $r \propto L^{0.25}$), this implies a UV LF with concave-upwards form at >-15 mag (see Figure 6). On the other hand, if one supposes one should recover a standard faint-end form for the UV LF, one must assume a steep size-luminosity relation, e.g., $r \propto L^{0.5}$. The observations do not appear to allow for the assumption of both (1) a conventional size-luminosity relation (with $r \propto L^{0.25}$) and (2) a conventional faint-end form for the UV LF at >-15 mag.

completeness measures, there are strong observational and theoretical reasons for disfavoring such a “concave-upwards” luminosity function. As demonstrated by Weisz et al. (2014) and Boyle-Kolchin et al. (2014, 2015), abundance matching of nearby dwarf galaxies sets a strong upper limit on the volume density of lower luminosity galaxies in the high-redshift universe.

From a theoretical perspective, one would expect the faint-end of the LF to trace the halo LF to some degree, but at the extreme faint end, the UV LF is expected to flatten or even turn over, as a result of increasingly inefficient gas cooling and radiative heating. A typical turn-over luminosity is ~ -12 mag (Liu et al. 2017; Finlator et al. 2015; Gnedin 2016; O’Shea et al. 2015; Ocvirk et al. 2016; Yue et al. 2016; Dayal et al. 2014). Theoretical LFs are not expected to become steeper towards the extreme low luminosity end.

If we discount such an upward change in the slope on the basis of these plausibility arguments, we must assume that the size-luminosity relation must show a break at ~ -17 mag, such that lower luminosity galaxies are all very small. This would translate to generally high levels of completeness in searches for lower luminosity galaxies. Bouwens et al. (2017b) made use of such small size assumptions in deriving constraints on $z \sim 6$ UV LF, finding a roughly fixed faint-end slope to very low luminosities >-14 mag, with a possible turn-over at the faint end. The best-fit $z \sim 6$ LF results of Bouwens et al. (2017b) are included in the right panel of Figure 6 with a black line.

In Bouwens et al. (2017a), we had provided an independent motivation for supposing that faint galaxy population is intrinsically small – and the observed size-luminosity relation is not predominantly driven by surface-brightness selection effects. That motivation is the approximately constant surface density of $z \sim 6-8$ sources in high-magnification regions behind clusters over a wide range of shear factors. This would only be the case if sources were intrinsically small, as larger intrinsic sizes would result in a much higher prevalence of sources in high-magnification regions with low shear factors. This is due to the fact that sources are readily detectable in low shear regions over a much larger range of sizes than is possible in regions around a lensing cluster with high shear.

As a caveat to this discussion, we should emphasize that the conclusions that we have drawn in this subsection are sensitive to the predictive power of the lensing models. If the lensing models lose their predictive power above magnification factors of ~ 10 , the sources that make up our nominally lowest luminosity samples (i.e., $M_{UV} > -15$ mag or $M_{UV} > -14$ mag) would instead be prominently made up of sources at higher intrinsic luminosities, i.e., $M_{UV} \sim -15$ mag, scattering to lower lower luminosities due to uncertainties in the lensing models. Despite this possibility, we emphasize that there is significant evidence that lensing models (especially the median model) maintain their predictive power to magnification factors of at least 20-30, if the tests run by Meneghetti et al. (2017), Prieuwe et al. (2017), or

Bouwens et al. (2017b) can be trusted.

The arguments presented in this section are subtle but clear and are summarized in Figure 7. If plausible luminosity functions are to be obtained at extremely low luminosities (i.e., > -15 mag), where plausible means “not upturning” (as predicted in most theoretical models: e.g., Dayal et al. 2014; Gnedin 2016; Liu et al. 2016), then such sources must be small. The use of sizes resulting from a simple extrapolation of the size-luminosity relation found for higher luminosity galaxies would suggest very large completeness corrections and imply an upturn. The clear implication is that there must be a break in the size-luminosity relation below ~ -17 mag to a steeper slope at lower luminosities.

5. DISCUSSION

5.1. Comparison with Previous Compilations of Small Star-Forming Sources

Before discussing the implications of the recovered size distribution for the sample of $z = 6-8$ galaxies we have identified, it is useful to reexamine the sample of very small ($\sim 10-100$ pc) sources identified by Vanzella et al. (2017a) using the current size measurements and also compare against new results recently obtained by Kawamata et al. (2017: which are an update to the earlier Kawamata et al. 2015 results).

Encouragingly, two of the three star-forming candidates that Vanzella et al. (2017a) identify over MACS0416 (the only HFF cluster analyzed both in the present study and that earlier study) are also included in our compilation of small sources (Table 2). M0416I-6115434445 corresponds to GC1 from Vanzella et al. (2017a), while M0416I-6114803434 corresponds to D1 from Vanzella et al. (2017a). We also have D2 from Vanzella et al. (2017a) in our source catalogs and so we can also compare our size and luminosity measurements for these sources.

For GC1, D1, and D2, we infer half-light radii of 21_{-13}^{+31} pc, 38_{-14}^{+21} pc, and 72_{-30}^{+39} pc vs. similar half-light radius measurements of 16 ± 7 pc, 140 ± 13 pc, and < 100 pc, respectively, from Vanzella et al. (2017a). The sizes we infer for M0416I-6115434445/GC1 and M0416I-6103003258/D2 are in excellent agreement with those from Vanzella et al. (2017a). For the third source M0416I-6114803434, the half-light radius we estimate is $3\times$ higher than the estimate from Vanzella et al. (2017a). This is almost certainly due to their fit giving a best-fit Sersic parameter of $n = 3.0 \pm 0.3$ (which results in a much larger half-light radius estimate). However, Vanzella et al. (2017a) do quote a 50-pc estimated size for the central high-surface brightness region of that source.

We also compare our size measurements with those from Kawamata et al. (2017), who have updated the results from Kawamata et al. (2015) to include sources from all six HFF clusters and parallel fields. Cross-matching our source catalogs with sources in the Ishigaki et al. (2017)/Kawamata et al. (2017) catalogs, we find 80 sources in common. In the median, our size measurements agree fairly well with those from Kawamata et al. (2017), with our measured sizes being $15 \pm 7\%$ larger. For individual sources, the differences are larger, with a 1σ scatter in our size estimates of 0.32 dex. For sources in common between our catalogs, when we estimate sizes

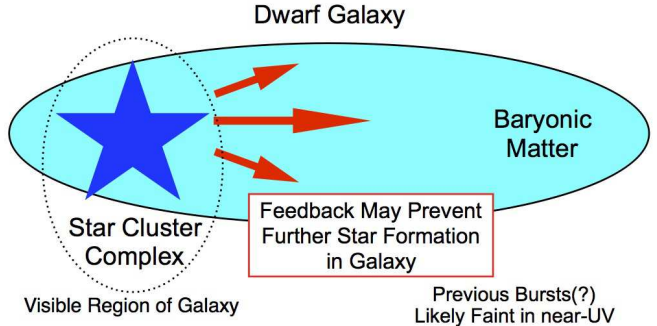


FIG. 8.— Cartoon schematic showing the formation of a single star cluster complex within a high-redshift dwarf galaxy. The star cluster forms out of overdense baryonic material. As feedback from the star cluster complex could temporarily inhibit star formation in other regions of the galaxy (e.g., Bastian 2008), galaxies may be much smaller in terms of their readily-visible spatial extent than they actually are. The spatial size of distant star-forming galaxies would also be made to look smaller than they are due to dominant impact of the youngest star cluster complexes on the UV morphologies of dwarf galaxies (e.g., Ma et al. 2017), as occurs e.g. in nearby tadpole galaxies (e.g. Kiso 5639: Elmegreen et al. 2016) or blue compact dwarf galaxies (Elmegreen et al. 2012b; Papaderos et al. 2008). In particular, Figures 4 and 5 of Elmegreen et al. (2016) would be strikingly similar to the compact objects seen at high redshift. The lensed $z \sim 5$ galaxy MS1358+62 (Franx et al. 1997), with a dominant star cluster complex < 200 pc in size (see Swinbank et al. 2009; Zitrin et al. 2011), also provides us with another dramatic example.

less than 50 pc, the median size measurement in their catalog is 35 pc. Similarly, when Kawamata et al. (2017) estimate sizes less than 50 pc, the median size measurement in our catalog is 62 pc. As such, there is reasonable agreement (at least in the median) between our estimated sizes and those of Kawamata et al. (2017) and also our selected samples of sources with small sizes and those of Kawamata et al. (2017). This is encouraging and increases our confidence in our results as we proceed to an interpretation.

5.2. Similarity of Lensed $z = 6-8$ Sources to Star Cluster Complexes in $z \sim 1-3$ Galaxies

As we discussed in §4.2 to §4.4, the ultra faint sources we identify at $z \sim 6-8$ behind the HFF clusters show significantly smaller sizes than the extrapolated size-luminosity relation for $z = 6-8$ galaxies from blank field studies. Interestingly, the size and luminosities of these sources lie in the general range of star cluster complexes identified in $z \sim 2-3$ galaxies, as presented earlier in Figure 1 in §3.2 (see also Figure 4). It is therefore logical to wonder if some of the sources we are identifying behind the HFF clusters may simply be star cluster complexes viewed at $z \sim 6-8$.

In some cases, it is possible that these sources correspond not simply to individual star cluster complexes but actually to super star clusters. It is difficult to be sure about a star cluster identification at the spatial resolutions available with HST (or ground-based telescopes) even with lensing magnification. Nevertheless, the small sizes, young ages, and almost identical redshifts to brighter nearby galaxies does make such an identification at least possible, as Vanzella et al. (2017b) do for several compact star-forming sources in the MACS0416 field.

Whatever the reality be for the smallest sources in our sample, it certainly seems plausible to make the connec-

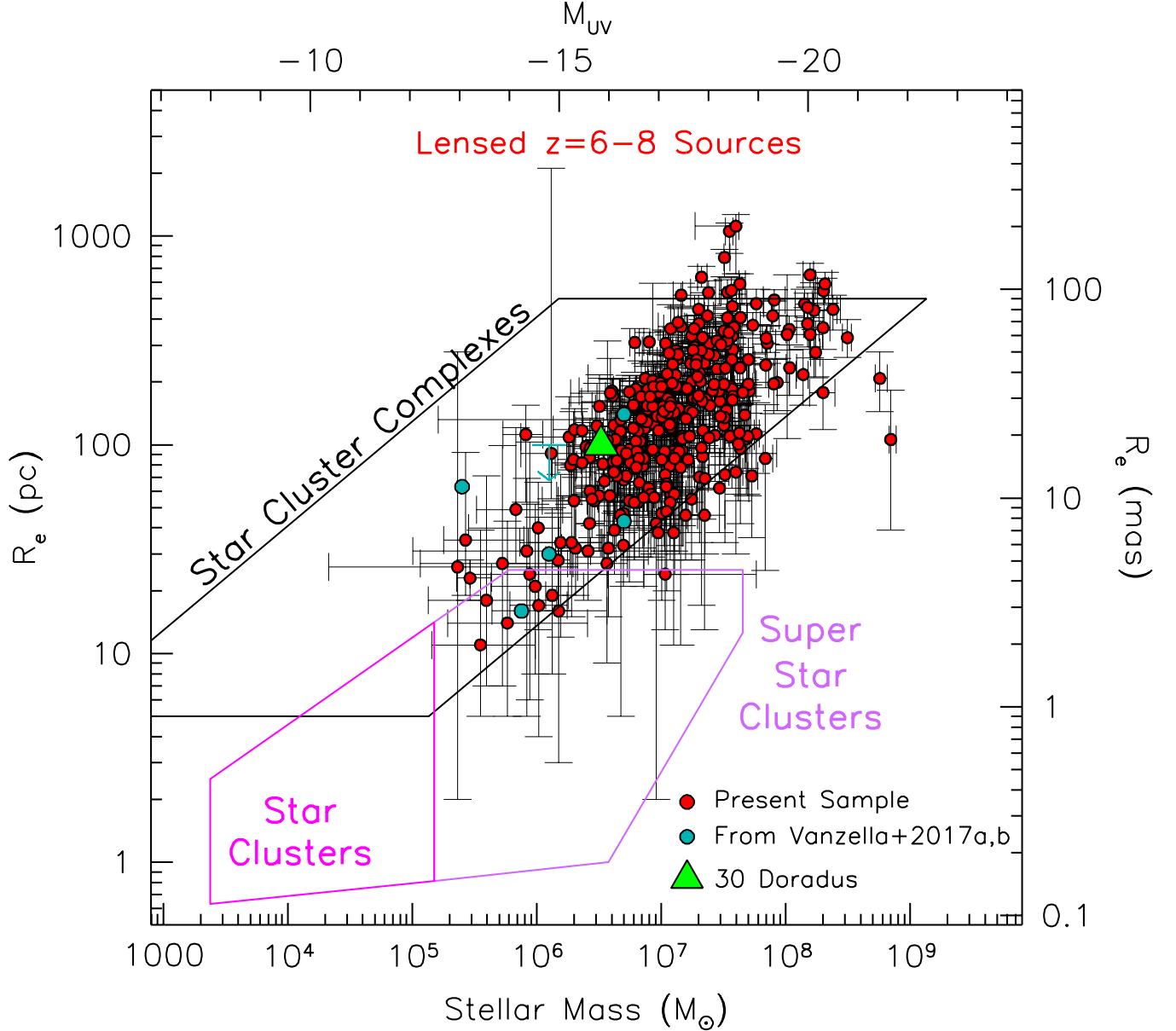


FIG. 9.— Comparison of the inferred sizes and luminosities of lensed galaxies in the HFF clusters (*red circles*) with star clusters (*demarcated by the magenta lines*: §3.3), super star clusters (*demarcated by the violet lines*: §3.3), and star cluster complexes (*demarcated by the black lines*: §3.2 and Figure 1). 1σ errors are the same as shown in Figure 4. The cyan circles show the sizes and luminosities reported by proto-globular clusters and star cluster candidates claimed by Vanzella et al. (2017a, 2017b) while the green triangle shows the size and luminosity of the 30 Doradus star complex. The conversion between a given UV luminosity and a stellar mass is made assuming a star formation duration of 10 Myr. While most of the lensed $z = 6-8$ sources in the HFF observations appear to have sizes and luminosities consistent with star cluster complexes seen in $z = 0-3$ galaxies (Bastian et al. 2006; Jones et al. 2010; Wisnioski et al. 2012; Swinbank et al. 2012; Livermore et al. 2012; Adamo et al. 2013; Livermore et al. 2015; Johnson et al. 2017; Dessauges-Zavadsky et al. 2017), a few sources lie in the star cluster regions. We use the few sources found in the star cluster region to place constraints on the volume density of proto-globular clusters at $z \sim 6$ (§5.4 and Figure 11).

tion of sources in our study to individual star cluster complexes. The sheer number of sources with ~ 100 pc sizes and luminosities similar to star cluster complexes makes the connection natural. The fact that the observed sizes of the sources are smaller than the relation seen for the brightest galaxies and from lower redshifts – where radius scales as $L^{1/4}$ or $L^{1/3}$ (e.g., de Jong & Lacey 2000; van der Wel et al. 2014) suggests we may not be seeing all the baryonic material associated with a given dwarf galaxy. Indeed, we are likely only observing a single dominant star cluster complex within each source. Consistent with

our suggested scenario, observations show an increasing fraction of the light in star cluster complexes, from low redshift to high redshift (Ribeiro et al. 2016).

How likely is it for lower-mass galaxies in the $z = 6-8$ universe to host just a single dominant star cluster complex? While addressing such a question would almost certainly require high resolution hydrodynamical simulations (e.g., see Ma et al. 2017), one could easily imagine the collapse of an overdensity resulting in the formation of a star cluster complex and feedback from that star cluster complex preventing star formation from

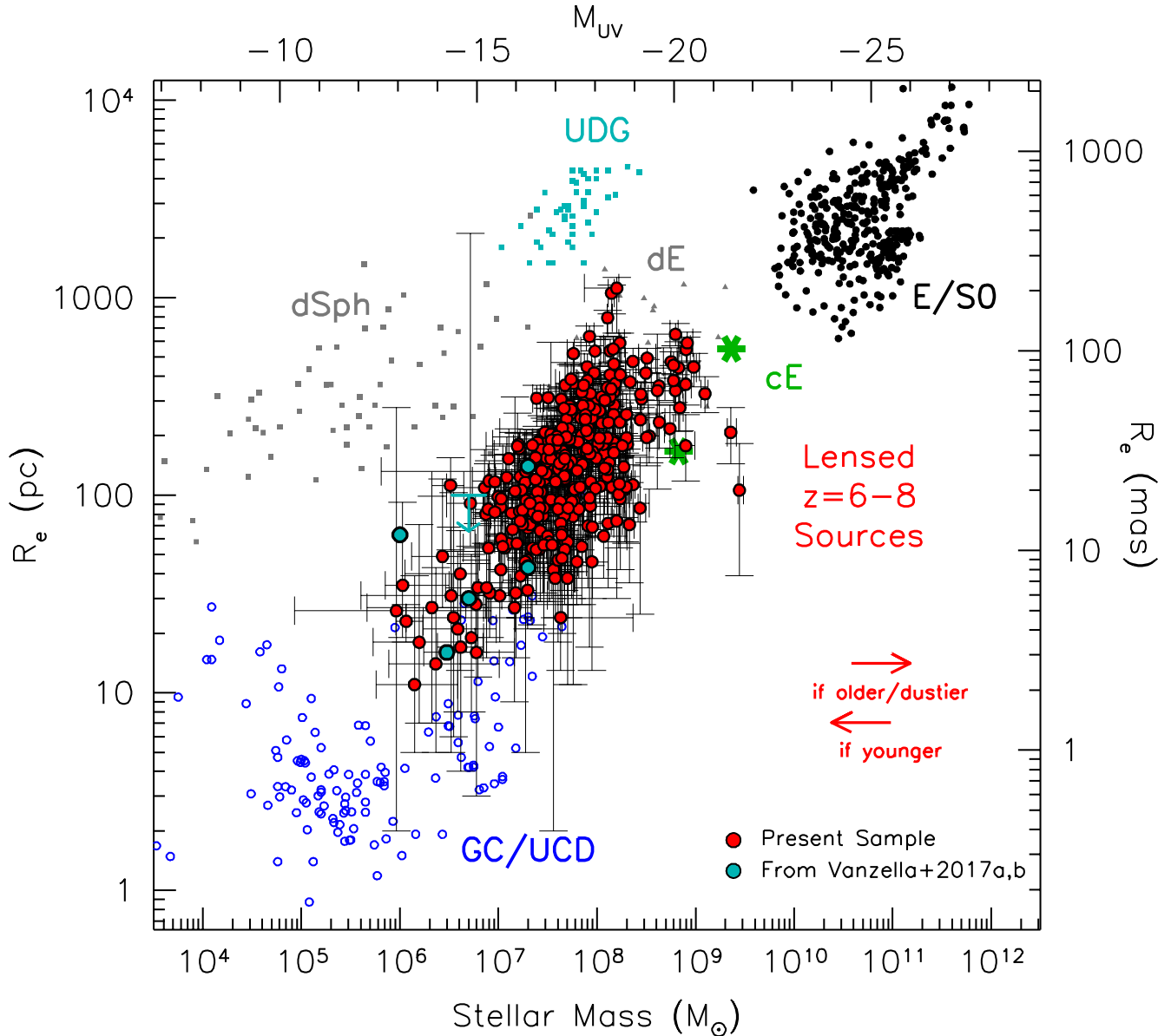


FIG. 10.— Similar to Figure 9, but focusing on comparisons with the sizes and masses of various evolved stellar systems in the nearby universe, including E/SO (*black circles*), ultra diffuse elliptical galaxies (*cyan squares*), dwarf spheroidals (dSphs: *gray squares*), dwarf ellipticals (dEs: *gray triangles*), compact ellipticals (cEs: *green star-like symbols*), and globular clusters/ultra compact dwarfs (*open blue circles*). The conversion between a given UV luminosity and a stellar mass is made assuming a star formation duration of 100 Myr. The left and right red arrows shows the expected change in the inferred masses when changing the duration of star formation from 100 Myr to 10 Myr and 400 Myr, respectively. The layout of this figure is similar to Figure 8 in Brodie et al. (2011) and Figures 11 of Norris et al. (2014). While the smallest lensed $z = 6-8$ sources in the HFF observations appear to have sizes / luminosities consistent with that of globular clusters / ultra-compact dwarfs, most of the lensed $z = 6-8$ galaxies have sizes and luminosities that lie in the region between globular clusters and that of elliptical galaxies and seem to best match that seen in star cluster complexes (Figure 9). They presumably undergo further dynamical evolution and/or accretion before becoming the evolved descendants we see today.

occurring at any other position in a dwarf galaxy (Figure 8). A simple calculation assuming SNe wind speeds of 50 km/s and a dwarf galaxy size of 200 pc suggests a feedback time of only 4 Myr, potentially a short enough time for starburst activity in one star cluster complex to regulate star formation across an entire dwarf galaxy (e.g., see Bastian 2008).

The discussion here and the match with local and lower-redshift star cluster complexes (discussed in the next section and shown in Figure 9) suggest that low-luminosity high-redshift $z \sim 6-8$ galaxies might be well-

described as having a single dominant star cluster complex. Such a star forming cluster complex does not, of course, preclude the galaxy itself from being larger (cf., the $z = 4.92$ Franx et al. (2017) MS1358+62 example) in terms of its physical extent, but the lower surface brightness regions could easily be missed in many sources due to cosmic surface brightness dimming (e.g., see Ma et al. 2017).

Based on the considerations from the previous section, it is already clear that some of the faint lensed sources in the HFFs could correspond to forming star cluster complexes in the distant universe, whether those star cluster complexes are the dominant (and only?) complex in a galaxy or whether those complexes are associated with a brighter system.

It is interesting to ask how the faint lensed sources we are finding compare with various stellar systems found in the nearby universe. For this exercise, we use the compilation that Norris et al. (2014) and M. Norris (2017, private communication) provide of the sizes and masses for a wide variety of local sources. This compilation includes elliptical galaxies (e.g., Cappellari et al. 2011; McDermid et al. 2015), ultra-diffuse elliptical galaxies (e.g., van Dokkum et al. 2015), dwarf ellipticals and spheroids (e.g., Misgeld et al. 2008), compact ellipticals such as Messier 32 (e.g., Chilingarian et al. 2009), ultra-compact dwarfs (e.g., Evstigneeva et al. 2007; Misgeld et al. 2011), and globular clusters (e.g., Hasegan et al. 2005; Firth et al. 2007; Mieske et al. 2007; Francis et al. 2012). The black and magenta lines indicate the region in parameter space where we would expect star cluster complexes and star clusters, respectively, to reside (§3.2-§3.3).

Figure 10 shows the inferred sizes and indicate masses for our lensed $z \sim 6$ -8 sample relative to the Norris et al. (2014) compilation. The indicative masses that we use for our lensed sample are computed assuming a fixed stellar population duration of 100 Myr in converting from their inferred UV luminosities M_{UV} .

Interestingly, some lensed sources in our samples have size and luminosities in the regime of ultra-compact dwarf galaxies or globular clusters, with measured sizes < 40 pc – as we previously remarked in §4.2-§4.4 and suggestively indicated by the magenta lines. Kawamata et al. (2015) had previously reported two sources with such small sizes. Now, thanks mostly to the present work and that by Kawamata et al. (2017) as well as a few candidates by Vanzella et al. (2017a, 2017b), we now know of a large number of very small star-forming sources in the distant universe.

While we must allow for the fact that some fraction of these high-redshift sources might be intrinsically larger than what we infer due to lensing uncertainties (see §4.4), it is likely that a modest fraction of these sources may genuinely be quite small. What therefore is the nature of these especially compact star-forming sources? A few could, in fact, correspond to proto-globular clusters or super star clusters, as Figure 9 illustrates (see also Vanzella et al. 2017a, 2017b). Nevertheless, we should emphasize that the bulk of our sample is more extended in size, suggesting that a more natural hypothesis is that most sources better match up with the properties of star cluster complexes.

5.4. Limits on the Volume Densities of Forming Globular Clusters in the $z \sim 6$ Universe

We can also use our size measurements of lensed sources behind the HFF clusters to set constraints on the luminosity function of proto-globular clusters in the early universe. As we remarked in the introduction, the large ages of stars in most globular clusters together with the high gas densities appropriate for globular cluster formation (Goddard et al. 2010; Adamo et al. 2011; Silva-

TABLE 3
VOLUME DENSITY CONSTRAINTS ON PROTO-GLOBULAR CLUSTERS FORMING AT $z \sim 6$

M_{UV}	ϕ (Mpc $^{-3}$)
This Work ^a	
-17.50	$< 0.00013^b$
-16.50	$< 0.00033^b$
-15.50	$< 0.013^b$
-14.50	$< 0.065^b$
-13.50	$< 0.068^b$
Estimated From Vanzella et al. (2017a)	
-15.50	$< 0.0106^{b,c}$
Volume Densities Probed with the HFF program ^d	
-17.50	0.00014
-16.50	0.00041
-15.50	0.0019
-14.50	0.0098
-13.50	0.054
-12.50	0.8

^a Fraction of sources which are measured to have a size of 40 pc or smaller multiplied by the volume density of sources in the Bouwens et al. (2017b) $z \sim 6$ LF

^b 1σ upper limits

^c We use the same criteria in establishing the upper limits on the proto-globular cluster volume densities as we use for our own observational results

^d Gray region in Figure 11

Villa & Larsen 2011) – as well as the high prevalence of globular clusters even in lower-mass galaxy halos (Spitler & Forbes 2009; Harris et al. 2013) – strongly suggest a $z \gtrsim 1.5$ formation era. Having observational constraints on the formation of these sources in the early universe is both valuable and interesting.

Given the proximity in time of powerful facilities like the James Webb Space Telescope JWST, there are now numerous predictions for the number of such clusters which might be found in a typical search field with the JWST (Renzini 2017; Boylan-Kolchin 2017a, 2017b; Elmegreen et al. 2012a) as well as candidate proto-globular clusters identified in separate studies (Vanzella et al. 2017a).

To provide constraints on the volume density of forming globular clusters in early universe, we explicitly consider the size constraints we have available for our full sample of $z \sim 6$ sources over the first four HFF clusters from this paper vs. that expected for star clusters (Figure 9). If the size measurements we have for a source yield a half-light radius measurement of < 40 pc, we consider it as a possible globular cluster candidate. We are, of course, aware that 40 pc is larger than the upper size limit on star clusters in the lower redshift universe, which is the range of 10-20 pc (§3.3), but we are considering a more inclusive selection here to ensure that both our selection and upper limits we set include the broadest range of possible candidates. Using this definition, one of the $z \sim 6$ sources with size measurements from Kawamata et al. (2015), i.e., HFF1C-i10, would qualify as a proto-globular cluster candidate.

In the upper panel of Figure 11, we present the fraction of $z \sim 6$ sources which could correspond to forming globular clusters vs. UV luminosity (i.e., those with $r_e \leq 40$ pc: see Table 2). We then show in the middle panel of Figure 11, the implied upper limits we can obtain on the

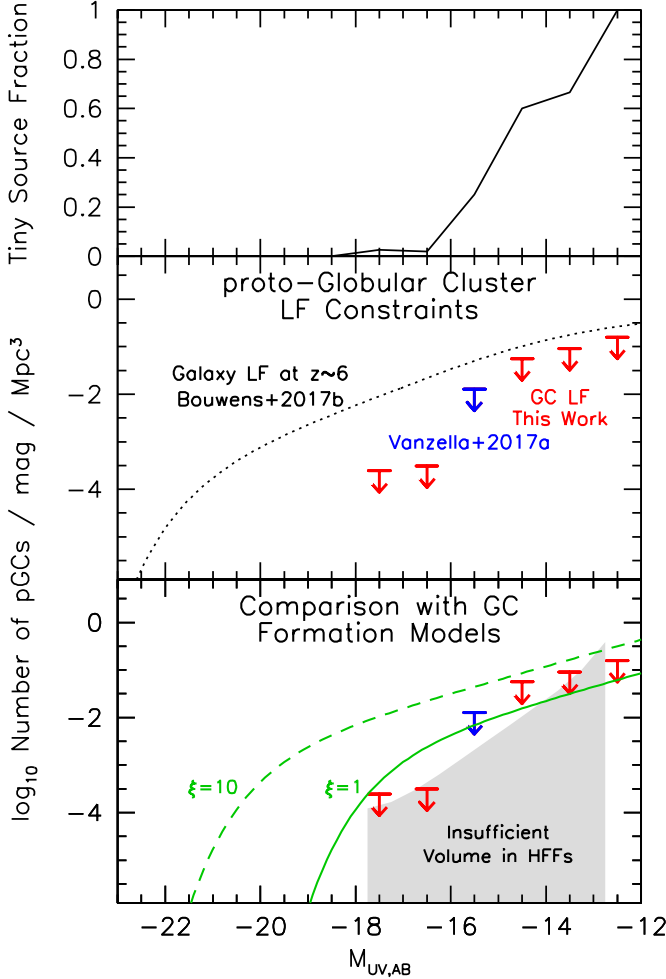


FIG. 11.— (*upper*) Fraction of the lensed $z \sim 6$ sources in the HFF observations which are measured to have half-light radii ≤ 40 pc. (*middle*) Constraints on the volume density of forming proto-globular clusters at $z \sim 6$ using searches for small sources behind the HFF clusters. The plotted red upper limits combine the UV LF constraints we obtained from the first four HFF clusters with the fraction of sources for which the available constraints suggest sizes ≤ 40 pc. The blue upper limit give the volume density constraints we infer here for the proto-globular cluster reported by Vanzella et al. (2017a). The dotted black line shows a recent determination of the $z \sim 6$ LF for galaxies from the Hubble Frontier Fields from Bouwens et al. (2017b) and which was used to derive the observational constraints (together with the results in the top panel). (*lower*) Comparison of the observational constraints on the proto globular cluster volume densities with the predicted LF of proto-globular cluster candidates from Boylan-Kolchin (2017a, 2017b) assuming the mass ratio $\xi = 1$ (*green solid line*: see §5.4) and $\xi = 10$ (*green dashed line*). The shaded gray region shows the volume densities and luminosities where the HFF program does not provide us with sufficient volume to probe; its upper envelope is equal to the reciprocal of the total volume computed to be available over the first six HFF clusters in the Bouwens et al. (2017, in prep) analysis.

volume density of proto-globular clusters forming in the distant universe. Given the challenges in being sure that any given system corresponds to a proto-globular cluster (or the challenges in being sure that specific lensed sources are in fact small: see §4.4), we include our constraints as upper limits. In the same panel, we also include the one proto-globular cluster candidate GC1 identified by Vanzella et al. (2017a) at $z \sim 6$ again as an upper limit on the volume density. For consistency with the

candidates included from our own study, we only include this candidate since its inferred size of 16 ± 7 pc satisfies our criterion of a source size < 40 pc. In Table 3, we provide the estimated upper limits on the volume density of sources for ready comparison.

For comparison with our proto-globular cluster constraints, we also include on Figure 11 the predicted number of proto-globular cluster and evolved globular cluster systems as a function of UV luminosity estimated to be present in the $z = 6-10$ universe using the model of Boylan-Kolchin (2017a, 2017b). Boylan-Kolchin (2017b) provide a convenient Schechter function approximation for this model globular cluster LF which we include in the figures. Shown are the predicted globular cluster LF for two different values for the ratio of mass in the initial globular cluster at its birth and that present at $z = 0$, i.e., $\langle m_{GC}(\text{birth}) \rangle / \langle m_{GC}(z = 0) \rangle$. Following Boylan-Kolchin (2017a, 2017b), we use the symbol ξ to describe this ratio and present both the $\xi = 1$ case (where $\phi^* = 4 \times 10^{-3} \text{ Mpc}^{-3}$, $M^* = -16.9$, $\alpha = -1.7$) and $\xi = 10$ case (where $\phi^* = 4 \times 10^{-3} \text{ Mpc}^{-3}$, $M^* = -19.4$, $\alpha = -1.7$) in Figure 11. The $\xi = 10$ case involves substantial mass loss after the initial globular burst would favor very bright proto-globular clusters in the early universe. Such a scenario is motivated e.g. by Schaerer & Charbonnel (2011) based on chemical complexity of the enrichment in globular clusters (see also D’Ercole et al. 2008; Renzini et al. 2015).

For context, we also show on Figure 11 the volume densities to which we would be able to search for proto-globular clusters of specific luminosities with the full HFF program. The volume densities are computed as in Bouwens et al. (2017b) and hence would be for a probe of proto-globular clusters at $z \sim 6$, but are based on the results over all six HFF clusters (Bouwens et al. 2017, in prep). These volume densities are also compiled in Table 3 for convenience. The search volume available for proto-globular clusters in the $z = 6-10$ universe is $\sim 3 \times$ larger.

Remarkably, the predictions of the $\xi = 1$ Boylan-Kolchin (2017a, 2017b) model lie very close to the upper limits we can set on the basis of existing HFF search results faintward of -16 mag. They are clearly in excess of our constraints over the HFFs brightward of -16 mag, predicting ~ 3 and ~ 10 sources at -17.5 mag and -16.5 mag, respectively, within the volume of the HFF program. Interestingly, at slightly fainter luminosities, i.e., -15.5 mag, our observational results (*red downward arrows*) are also much more consistent with the minimal $\xi = 1$ scenario sketched out by Boylan-Kolchin (2017a: *green solid line*). If the Boylan-Kolchin (2017a) $\xi = 1$ scenario is correct, three -15.5 -mag sources identified with the HFF program are expected to correspond to proto-globular clusters in formation. While a small number, these constitute $\sim 50\%$ of the tiny star-forming sources that we have identified at those low luminosities. These results indicate that we observe plausible consistency between the $\xi = 1$ model of Boylan-Kolchin (2017a) and what we derive from our size and LF results.

Interestingly, and rather definitively, the $\xi = 10$ model of Boylan-Kolchin (2017a) exceeds the upper limits we can set from the HFF observations at all luminosities. As such, we can probably already rule the $\xi = 10$ model out

(unless proto-globular clusters are lost within the light from their host galaxy). This adds to other independent evidence against such models (Bastian & Lardo 2015; Kruijssen 2015; Webb & Leigh 2015; Martocchia et al. 2017; Elmegreen 2017).

This suggests that observers may be on the brink of exploring the formation of globular clusters in the distant universe with current and especially using future observations with JWST (see also discussion in Renzini 2017). With JWST, not only will be able to search for proto-globular cluster candidates much more efficiently, but we will be able to characterize each candidate system in detail using high S/N spectroscopy, probing the velocity dispersion (and thus allowing for a measurement of the dynamical mass) as well as the chemical maturity of such systems.

6. SUMMARY

Here we make use of the unique depth and resolving power of the HFF cluster observations to examine the sizes and luminosities of 153 $z \sim 6$, 101 $z \sim 7$, and 53 $z \sim 8$ sources identified in the early universe behind the first four HFF clusters (307 $z = 6-8$ galaxies in total). We restricted ourselves to an analysis of sources behind the first four HFF clusters since those possess the most mature lensing models leveraging substantial spectroscopic redshift constraints and a substantial number of multiple image systems.

The depth of the HFF observations and the lensing from the massive foreground clusters make it possible for us to measure the sizes for ~ -18 mag and ~ -15 mag galaxies to a typical 1σ accuracy of ~ 50 pc and ~ 10 pc, respectively. Achieving such high accuracy on size measurements is crucial for distinguishing between normal galaxies, star cluster complexes, star clusters, and even proto-globular clusters forming in the early universe.

To obtain the most robust measurements on the sizes and luminosities of sources, we make use a MCMC procedure to fit the available imaging data for each source (§4.1). We also utilize the median magnification and shear factors derived from six different varieties of parametric lensing models CATS, Sharon/Johnson, GLAFIC, Zitrin-NFW, Keeton, and Caminha. The model profile is lensed according to the median magnification and shear factor, convolved with the PSF, and then compared with a stack of the available WFC3/IR data on each source.

The measured sizes of lensed $z = 6-8$ galaxies in our sample trend with UV luminosity L approximately as $L^{0.5 \pm 0.1}$ (Figure 4: see §4.2) at > -17 mag, reaching sizes of 11_{-6}^{+28} pc. This is shallower than the trend for more luminous (< -18 mag) sources, i.e., $r \propto L^{0.26 \pm 0.03}$, suggesting a break in the relation at ~ -17 mag. While the trend we recover at lower luminosity is similar to what one might expect as a result of surface brightness selection effects (e.g., Bouwens et al. 2017a; Ma et al. 2017), our lowest luminosity samples show no particular evidence for being especially incomplete. If one assumes the lowest luminosity sources have small sizes (and hence minimal completeness corrections), one derives plausible LF results, as we demonstrated in Bouwens et al. (2017b) for the $z \sim 6$ LF. If one however adopts a much shallower size-luminosity relation – as found by Shibuya et al. (2015) to holds for the lower-redshift star-forming

galaxies and the brightest high-redshift sources – high-redshift selections would become appreciably incomplete at > -15 mag and the inferred LFs would show a concave-upwards form at > -15 mag (see §4.4). This situation is summarized in Figures 6 and 7.

Sources in our lensed $z = 6-8$ samples have measured sizes and luminosities which are very similar to that derived for star cluster complexes identified in galaxies at $z = 0-3$ (Jones et al. 2010; Livermore et al. 2012, 2015; Wisnioski et al. 2012; Swinbank et al. 2012; Johnson et al. 2017). In fact, the typical -15 mag galaxy in our samples has a smaller half-light radius than 30 Doradus, which has a measured half-light radius of ~ 100 pc. This could be interpreted to suggest that lower luminosity galaxies in the early universe may often contain a single prominent star cluster complexes which dominates the observed UV morphology.

The impact that errors in the gravitational lensing models would have on our results is considered using sophisticated simulations (§4.3) similar to that used in our previous work on the $z \sim 6$ LF. The results of the simulations suggest that some fraction of the compact star-forming sources identified in our fields actually have larger physical sizes and are simply inferred to be small, due to errors in the estimated lensing magnification. Results from these simulations also show fewer compact sources than we recover in the actual observations, suggesting that a fraction of the small sources we identify are bona-fide.

We also place the measured size and luminosities of lensed $z = 6-8$ galaxies in our samples with the sizes and masses of stellar systems in the nearby universe (§5.3). Most of the sources have inferred masses and luminosities that place them in the region of parameter space where star cluster complexes lie (§5.2), which occurs midway between ultra-compact dwarfs and elliptical galaxies. This suggests that many low-luminosity galaxies may be dominated by a single star cluster complex in terms of their observed morphologies. Nevertheless, we remark that for a small minority of sources in our sample, their properties are consistent with potentially corresponding to super star clusters and – as such – they could correspond to proto-globular clusters (Figure 10: see §5.3).

We combine current constraints on the fraction of especially small sources behind the HFF clusters with new state-of-the-art constraints on the UV LF of sources at $z \sim 6$ from the HFF clusters (Bouwens et al. 2017b) to derive constraints on the proto-globular cluster LF at high redshift (§5.4). Comparing this LF with predictions from the recent models from Boylan-Kolchin (2017a, 2017b: but see also Renzini 2017), we find that with current observations from the HFF clusters we are probably very close to identifying bona-fide globular clusters in formation in the early universe (if such sources have not been identified already with our probe or that of Vanzella et al. 2017a, 2017b).

For example, the $\xi = 1$ model of Boylan-Kolchin (2017a) suggests that ~ 3 , ~ 10 , and ~ 3 proto-globular clusters in formation should be visible in the HFF observations at -17.5 mag, -16.5 mag, and -15.5 mag. Tantalizing enough, while our observational results strongly disfavor objects with proto-globular cluster sizes at < -16 mag (see lowest panel of Figure 11), our results are plausibly consistent with this model faintward of -16 mag,

and in fact this model would suggest that 50% of the smallest sources in our -15.5 mag selection could correspond to proto-globular clusters.

Despite plausible consistency of our results with the most basic globular cluster formation models of Boylan-Kolchin (2017a), our observational results already place strong constraints on more extreme globular cluster formation scenarios, e.g., with $\xi = 10$, ruling out those scenarios entirely unless the forming star clusters cannot be picked out amongst the other light in their host galaxy halo (see also Bastian & Lardo 2015; Kruijssen 2015; Webb & Leigh 2015; Martocchia et al. 2017 for further evidence).

As in our previous work (Bouwens et al. 2017a) and in other work identifying especially compact sources in the distant universe (Vanzella et al. 2017a, 2017b), we caution that the present conclusions depend on the parametric lensing models having predictive power to magnification factors of ~ 20 – which appears quite likely given the results of e.g. Meneghetti et al. 2017, Bouwens et al. 2017b, and Appendix A.

In the future, we plan to extend the present analysis by looking at the sizes and luminosities of star-forming sources at $z = 2-5$ behind the HFF clusters as well as the $z = 6-8$ galaxies behind the final two HFF clusters when refined public magnification models are available. Compact star-forming sources identified behind the HFFs represent compelling targets for spec-

troscopy with both MUSE and JWST to gain more insight into the nature of these sources.

We acknowledge stimulating discussions with Angela Adamo, Nate Bastian, Mike Boylan-Kolchin, James Bullock, Rob Crain, Bruce Elmegreen, Phil Hopkins, Xiaocheng Ma, Mike Norman, Elliot Quataert, Alvio Renzini, Britton Smith, Eros Vanzella, Dan Weisz, Shelley Wright, and Tom Zick. Nate Bastian and Angela Adamo provided us with extremely valuable feedback on the scientific content and language used in this paper, especially with regard to star clusters and star cluster complexes. We are grateful to Mark Norris for sending us a compilation of the sizes, luminosities, and masses of many evolved stellar systems in the nearby universe. This work utilizes gravitational lensing models produced by PIs Bradač, Natarajan & Kneib (CATS), Merten & Zitrin, Sharon, and Williams, and the GLAFIC and Diego groups. This lens modeling was partially funded by the HST Frontier Fields program conducted by STScI. STScI is operated by the Association of Universities for Research in Astronomy, Inc. under NASA contract NAS 5-26555. The lens models were obtained from the Mikulski Archive for Space Telescopes (MAST). We acknowledge the support of NASA grants HST-AR-13252, HST-GO-13872, HST-GO-13792, and NWO grants 600.065.140.11N211 (vrij competitie) and TOP grant TOP1.16.057.

REFERENCES

- Adamo, A., Östlin, G., & Zackrisson, E. 2011, *MNRAS*, 417, 1904
 Adamo, A., Östlin, G., Bastian, N., et al. 2013, *ApJ*, 766, 105
 Alavi, A., Siana, B., Richard, J., et al. 2016, *ApJ*, 832, 56
 Atek, H., Richard, J., Jauzac, M., et al. 2015, *ApJ*, 814, 69
 Bastian, N., Gieles, M., Efremov, Y. N., & Lamers, H. J. G. L. M. 2005, *A&A*, 443, 79
 Bastian, N., Emsellem, E., Kissler-Patig, M., & Maraston, C. 2006, *A&A*, 445, 471
 Bastian, N. 2008, *MNRAS*, 390, 759
 Bastian, N., Schweizer, F., Goudfrooij, P., Larsen, S. S., & Kissler-Patig, M. 2013, *MNRAS*, 431, 1252
 Bastian, N., & Lardo, C. 2015, *MNRAS*, 453, 357
 Beckwith, S. V. W., Stiavelli, M., Koekemoer, A. M., et al. 2006, *AJ*, 132, 1729
 Bertin, E. and Arnouts, S. 1996, *A&AS*, 117, 39
 Bouwens, R. J., Illingworth, G. D., Blakeslee, J. P., Broadhurst, T. J., & Franx, M. 2004, *ApJ*, 611, L1
 Bouwens, R. J., Illingworth, G. D., Oesch, P. A., et al. 2011, *ApJ*, 737, 90
 Bouwens, R. J., Illingworth, G. D., Oesch, P. A., et al. 2014, *ApJ*, 793, 115
 Bouwens, R. J., Illingworth, G. D., Oesch, P. A., et al. 2017a, *ApJ*, 843, 41
 Bouwens, R. J., Oesch, P. A., Illingworth, G. D., Ellis, R. S., & Stefanon, M. 2017b, *ApJ*, 843, 129
 Boylan-Kolchin, M., Bullock, J. S., & Garrison-Kimmel, S. 2014, *MNRAS*, 443, L44
 Boylan-Kolchin, M., Weisz, D. R., Johnson, B. D., et al. 2015, *MNRAS*, 453, 1503
 Boylan-Kolchin, M. 2017a, *MNRAS*, 472, 3120
 Boylan-Kolchin, M. 2017b, *MNRAS*, submitted, arXiv:1711.00009
 Bradač, M., Treu, T., Applegate, D., et al. 2009, *ApJ*, 706, 1201
 Brammer, G. B., van Dokkum, P. G., & Coppi, P. 2008, *ApJ*, 686, 1503
 Brodie, J. P., & Strader, J. 2006, *ARA&A*, 44, 193
 Brodie, J. P., Romanowsky, A. J., Strader, J., & Forbes, D. A. 2011, *AJ*, 142, 199
 Cabrera-Ziri, I., Bastian, N., Davies, B., et al. 2014, *MNRAS*, 441, 2754
 Cabrera-Ziri, I., Bastian, N., Hilker, M., et al. 2016, *MNRAS*, 457, 809
 Caminha, G. B., Grillo, C., Rosati, P., et al. 2016, *A&A*, 587, A80
 Caminha, G. B., Grillo, C., Rosati, P., et al. 2017, *A&A*, 600, A90
 Cappellari, M., Emsellem, E., Krajnović, D., et al. 2011, *MNRAS*, 413, 813
 Castellano, M., Yue, B., Ferrara, A., et al. 2016, *ApJ*, 823, L40
 Coe, D., Bradley, L., & Zitrin, A. 2015, *ApJ*, 800, 84
 Dayal, P., Ferrara, A., Dunlop, J. S., & Pacucci, F. 2014, *MNRAS*, 445, 2545
 de Jong, R. S., & Lacey, C. 2000, *ApJ*, 545, 781
 D’Ercole, A., Vesperini, E., D’Antona, F., McMillan, S. L. W., & Recchi, S. 2008, *MNRAS*, 391, 825
 Dessauges-Zavadsky, M., Schaerer, D., Cava, A., Mayer, L., & Tamburello, V. 2017, *ApJ*, 836, L22
 Diego, J. M., Broadhurst, T., Molnar, S. M., Lam, D., & Lim, J. 2015, *MNRAS*, 447, 3130
 Diego, J. M., Broadhurst, T., Zitrin, A., et al. 2015, *MNRAS*, 451, 3920
 Diego, J. M., Broadhurst, T., Chen, C., et al. 2016, *MNRAS*, 456, 356
 Diego, J. M., Broadhurst, T., Wong, J., et al. 2016, *MNRAS*, 459, 3447
 Diego, J. M., Schmidt, K. B., Broadhurst, T., et al. 2016, *MNRAS*, submitted, arXiv:1609.04822
 Ellis, R. S., McLure, R. J., Dunlop, J. S., et al. 2013, *ApJ*, 763, L7
 Elmegreen, B. G., Malhotra, S., & Rhoads, J. 2012a, *ApJ*, 757, 9
 Elmegreen, B. G., Zhang, H.-X., & Hunter, D. A. 2012b, *ApJ*, 747, 105
 Elmegreen, D. M., Elmegreen, B. G., Sánchez Almeida, J., et al. 2016, *ApJ*, 825, 145
 Elmegreen, B. G. 2017, *ApJ*, 836, 80
 English, J., & Freeman, K. C. 2003, *AJ*, 125, 1124
 Evstigneeva, E. A., Drinkwater, M. J., Jurek, R., et al. 2007, *MNRAS*, 378, 1036
 Faber, S. M. 1973, *ApJ*, 179, 423
 Ferguson, H. C., Dickinson, M., Giavalisco, M., et al. 2004, *ApJ*, 600, L107

- Finlator, K., Thompson, R., Huang, S., et al. 2015, *MNRAS*, 447, 2526
- Firth, P., Drinkwater, M. J., Evstigneeva, E. A., et al. 2007, *MNRAS*, 382, 1342
- Fisher, D. B., Glazebrook, K., Damjanov, I., et al. 2017, *MNRAS*, 464, 491
- Forbes, D. A., & Bridges, T. 2010, *MNRAS*, 404, 1203
- Franx, M., Illingworth, G. D., Kelson, D. D., van Dokkum, P. G., & Tran, K.-V. 1997, *ApJ*, 486, L75
- Francis, K. J., Drinkwater, M. J., Chilingarian, I. V., Bolt, A. M., & Firth, P. 2012, *MNRAS*, 425, 325
- Gnedin, N. Y. 2016, *ApJ*, 825, L17
- Goddard, Q. E., Bastian, N., & Kennicutt, R. C. 2010, *MNRAS*, 405, 857
- Graus, A. S., Bullock, J. S., Boylan-Kolchin, M., & Weisz, D. R. 2016, *MNRAS*, 456, 477
- Grazian, A., Castellano, M., Koekemoer, A. M., et al. 2011, *A&A*, 532, A33
- Grazian, A., Castellano, M., Fontana, A., et al. 2012, *A&A*, 547, A51
- Harris, W. E., Harris, G. L. H., & Alessi, M. 2013, *ApJ*, 772, 82
- Haşegan, M., Jordán, A., Côté, P., et al. 2005, *ApJ*, 627, 203
- Holwerda, B. W., Bouwens, R., Oesch, P., et al. 2015, *ApJ*, 808, 6
- Huang, K.-H., Ferguson, H. C., Ravindranath, S., & Su, J. 2013, *ApJ*, 765, 68
- Illingworth, G. D., Magee, D., Oesch, P. A., et al. 2013, *ApJS*, 209, 6
- Ishigaki, M., Kawamata, R., Ouchi, M., et al. 2015, *ApJ*, 799, 12
- Ishigaki, M., Kawamata, R., Ouchi, M., Oguri, M., & Shimasaku, K. 2017, *ApJ*, submitted, arXiv:1702.04867
- Jauzac, M., Jullo, E., Eckert, D., et al. 2015a, *MNRAS*, 446, 4132
- Jauzac, M., Richard, J., Jullo, E., et al. 2015b, *MNRAS*, 452, 1437
- Jauzac, M., Richard, J., Limousin, M., et al. 2016, *MNRAS*, 457, 2029
- Johnson, T. L., Sharon, K., Bayliss, M. B., et al. 2014, *ApJ*, 797, 48
- Johnson, T. L., Rigby, J. R., Sharon, K., et al. 2017, arXiv:1707.00706
- Jones, T. A., Swinbank, A. M., Ellis, R. S., Richard, J., & Stark, D. P. 2010, *MNRAS*, 404, 1247
- Jullo, E., & Kneib, J.-P. 2009, *MNRAS*, 395, 1319
- Lada, C. J., & Lada, E. A. 2003, *ARA&A*, 41, 57
- Lagattuta, D. J., Richard, J., Clément, B., et al. 2017, *MNRAS*, 469, 3946
- Lam, D., Broadhurst, T., Diego, J. M., et al. 2014, *ApJ*, 797, 98
- Laporte, N., Infante, L., Troncoso Iribarren, P., et al. 2016, *ApJ*, 820, 98
- Liesenborgs, J., De Rijcke, S., & Dejonghe, H. 2006, *MNRAS*, 367, 1209
- Limousin, M., Richard, J., Jullo, E., et al. 2016, *A&A*, 588, A99
- Liu, C., Mutch, S. J., Poole, G. B., et al. 2017, *MNRAS*, 465, 3134
- Liu, C., Mutch, S. J., Angel, P. W., et al. 2016, *MNRAS*, 462, 235
- Livermore, R. C., Jones, T., Richard, J., et al. 2012, *MNRAS*, 427, 688
- Livermore, R. C., Jones, T. A., Richard, J., et al. 2015, *MNRAS*, 450, 1812
- Livermore, R., Finkelstein, S., Lotz, J. 2017, *ApJ*, 835, 113
- Lotz, J. M., Koekemoer, A., Coe, D., et al. 2017, *ApJ*, 837, 97
- Kawamata, R., Ishigaki, M., Shimasaku, K., Oguri, M., & Ouchi, M. 2015, *ApJ*, 804, 103
- Kawamata, R., Oguri, M., Ishigaki, M., Shimasaku, K., & Ouchi, M. 2016, *ApJ*, 819, 114
- Kawamata, R., Ishigaki, M., Shimasaku, K., et al. 2017, *ApJ*, submitted, arXiv:1710.07301
- Keeton, C. R. 2010, *General Relativity and Gravitation*, 42, 2151
- Kennicutt, R. C., Jr., Armus, L., Bendo, G., et al. 2003, *PASP*, 115, 928
- Kravtsov, A. V. 2013, *ApJ*, 764, L31
- Kruijssen, J. M. D. 2014, *Classical and Quantum Gravity*, 31, 244006
- Kruijssen, J. M. D. 2015, *MNRAS*, 454, 1658
- Ma, X., Hopkins, P. F., Boylan-Kolchin, M., et al. 2017, *MNRAS*, arXiv:1710.00008
- Mahler, G., Richard, J., Clément, B., et al. 2017, *MNRAS*, submitted, arXiv:1702.06962
- Maraston, C., Bastian, N., Saglia, R. P., et al. 2004, *A&A*, 416, 467
- Martocchia, S., Bastian, N., Usher, C., et al. 2017, *MNRAS*, 468, 3150
- McDermid, R. M., Alatalo, K., Blitz, L., et al. 2015, *MNRAS*, 448, 3484
- McLure, R. J., Dunlop, J. S., Bowler, R. A. A., et al. 2013, *MNRAS*, 432, 2696
- Meneghetti, M., Natarajan, P., Coe, D., et al. 2017, *MNRAS*, 472, 3177
- Merlin, E., Amorín, R., Castellano, M., et al. 2016, *A&A*, 590, A30
- Meurer, G. R., Heckman, T. M., Leitherer, C., et al. 1995, *AJ*, 110, 2665
- Mieske, S., Hilker, M., Jordán, A., Infante, L., & Kissler-Patig, M. 2007, *A&A*, 472, 111
- Misgeld, I., Mieske, S., & Hilker, M. 2008, *A&A*, 486, 697
- Misgeld, I., Mieske, S., Hilker, M., et al. 2011, *A&A*, 531, A4
- Mosleh, M., Williams, R. J., Franx, M., et al. 2012, *ApJ*, 756, L12
- Murray, N. 2009, *ApJ*, 691, 946
- Norris, M., Kannappan, S., Forbes, D. A., et al. 2014, *MNRAS*, arXiv:1406.6065v1
- Ocvirk, P., Gillet, N., Shapiro, P. R., et al. 2016, *MNRAS*, 463, 1462
- Oesch, P. A., Bouwens, R. J., Illingworth, G. D., et al. 2010a, *ApJ*, 709, L16
- Oesch, P. A., Bouwens, R. J., Illingworth, G. D., et al. 2015, *ApJ*, 808, 104
- Oguri, M. 2010, *PASJ*, 62, 1017
- Oke, J. B., & Gunn, J. E. 1983, *ApJ*, 266, 713
- Ono, Y., Ouchi, M., Curtis-Lake, E., et al. 2013, *ApJ*, 777, 155
- Owers, M. S., Randall, S. W., Nulsen, P. E. J., et al. 2011, *ApJ*, 728, 27
- Peng, C. Y., Ho, L. C., Impey, C. D., & Rix, H.-W. 2002, *AJ*, 124, 266
- Planck Collaboration, Ade, P. A. R., Aghanim, N., et al. 2015, arXiv:1502.01589 [PC15]
- Postman, M., Coe, D., Benítez, N., et al. 2012, *ApJS*, 199, 25
- Priewe, J., Williams, L. L. R., Liesenborgs, J., Coe, D., & Rodney, S. A. 2016, *MNRAS*, submitted, arXiv:1605.07621
- Rejkuba, M., Dubath, P., Minniti, D., & Meylan, G. 2007, *A&A*, 469, 147
- Renzini, A., D'Antona, F., Cassisi, S., et al. 2015, *MNRAS*, 454, 4197
- Renzini, A. 2017, *MNRAS*, 469, L63
- Rodríguez-Zaurín, J., Arribas, S., Monreal-Ibero, A., et al. 2011, *A&A*, 527, A60
- Ribeiro, B., Le Fèvre, O., Cassata, P., et al. 2016, *A&A*, submitted, arXiv:1611.05869
- Richard, J., Jauzac, M., Limousin, M., et al. 2014, *MNRAS*, 444, 268
- Schaerer, D., & Charbonnel, C. 2011, *MNRAS*, 413, 2297
- Schmidt, K. B., Treu, T., Trenti, M., et al. 2014, *ApJ*, 786, 57
- Sebesta, K., Williams, L. L. R., Mohammed, I., Saha, P., & Liesenborgs, J. 2016, *MNRAS*, 461, 2126
- Shibuya, T., Ouchi, M., & Harikane, Y. 2015, *ApJS*, 219, 15
- Silva-Villa, E., & Larsen, S. S. 2011, *A&A*, 529, A25
- Simon, J. D., & Geha, M. 2007, *ApJ*, 670, 313
- Spitler, L. R., & Forbes, D. A. 2009, *MNRAS*, 392, L1
- Swinbank, A. M., Webb, T. M., Richard, J., et al. 2009, *MNRAS*, 400, 1121
- Swinbank, A. M., Smail, I., Sobral, D., et al. 2012, *ApJ*, 760, 130
- Taghizadeh-Popp, M., Fall, S. M., White, R. L., & Szalay, A. S. 2015, *ApJ*, 801, 14
- van der Wel, A., Franx, M., van Dokkum, P. G., et al. 2014, *ApJ*, 788, 28
- van Dokkum, P. G., Abraham, R., Merritt, A., et al. 2015, *ApJ*, 798, L45
- Vanzella, E., Fontana, A., Zitrin, A., et al. 2014, *ApJ*, 783, L12
- Vanzella, E., Calura, F., Meneghetti, M., et al. 2017a, *MNRAS*, 467, 4304
- Vanzella, E., Castellano, M., Meneghetti, M., et al. 2017b, *ApJ*, 842, 47
- Vanzi, L., Cresci, G., Telles, E., & Melnick, J. 2008, *A&A*, 486, 393
- Webb, J. J., & Leigh, N. W. C. 2015, *MNRAS*, 453, 3278
- Weisz, D. R., Johnson, B. D., & Conroy, C. 2014, *ApJ*, 794, L3
- Wisnioski, E., Glazebrook, K., Blake, C., et al. 2012, *MNRAS*, 422, 3339

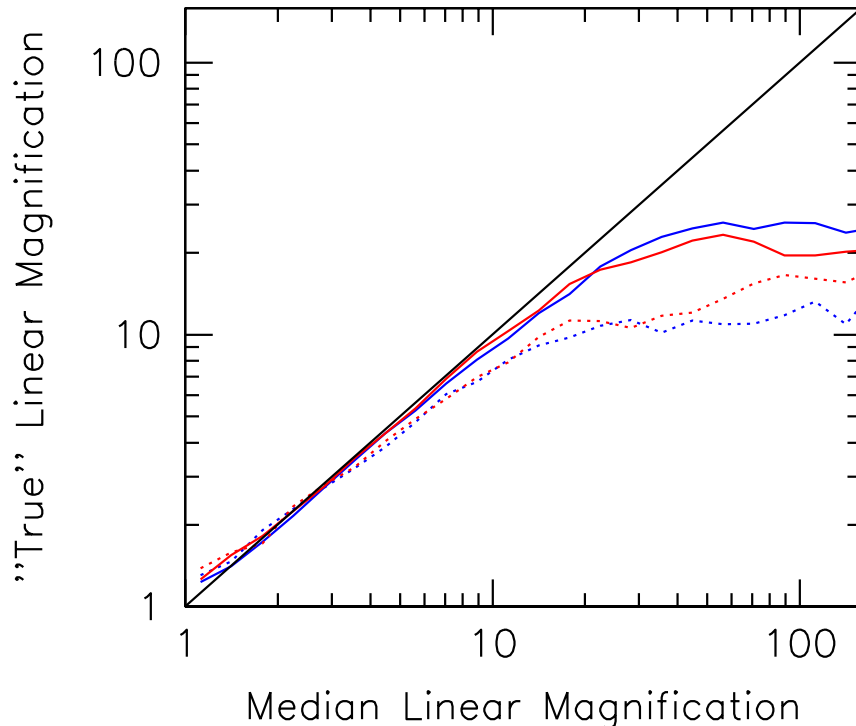


FIG. 12.— An illustration of how well the median linear magnification factor likely predicts the actual linear magnification factor. The plotted solid lines show the median of the linear magnification factor from the individual parametric models as a function of the median linear magnification factor for Abell 2744 (*red*) and MACS0416 (*blue*). The dotted lines show the relationship, if the median linear magnification factor from the parametric models is compared against the median magnification factor from the non-parametric models. The solid black line is shown for comparison to indicate the relationship that would be present for perfect predictive power for the lensing models. The linear magnification factors appear to have predictive power to factors of ~ 20 if we assume that the parametric lensing models are taken to represent a plausible representation of the actual lensing model and ~ 10 if we assume that the non-parametric models are. This figure is similar in form to Figure 3 from Bouwens et al. (2017b), though that figure is for the total magnification factor.

Yue, B., Ferrara, A., & Xu, Y. 2016, arXiv:1604.01314
 Zitrin, A., Broadhurst, T., Coe, D., et al. 2011, MNRAS, 413,
 1753
 Zitrin, A., Broadhurst, T., Bartelmann, M., et al. 2012, MNRAS,
 423, 2308

Zitrin, A., Meneghetti, M., Umetsu, K., et al. 2013, ApJ, 762, L30
 Zitrin, A., Fabris, A., Merten, J., et al. 2015, ApJ, 801, 44

APPENDIX

A. MAXIMUM LINEAR MAGNIFICATION FACTORS TO WHICH THE LENSING MODELS APPEARS TO BE RELIABLE

While magnification models appear to perform quite well in estimating the true magnification factors behind lensing clusters (Meneghetti et al. 2017) in the median, these models have difficulty in predicting the magnification factors very close to the critical curves. In the high-magnification regions, the model magnification factors tend to overpredict the actual magnification factors quite significantly (e.g., see Figure 3 from Bouwens et al. 2017b), e.g., at $\mu \gtrsim 30$.

For the present analysis of sizes, the principal quantity of interest is not the overall magnification factor, but rather the magnification along a single spatial dimension. While the linear magnification factor was not explicitly considered in the previous analyses of Meneghetti et al. (2017) and Bouwens et al. (2017), it should broadly correlate with the predictive power of the model magnification factors.

We can quantify the linear magnification factors to which our size measurements are reliable in the same way we previously determined the total magnification factors to which our lensing maps were sufficiently predictive of the total magnification factors (Bouwens et al. 2017b). As in that work, we alternatively treat one of the models as if it represented reality and investigated to what extent the median linear magnification factors from the other models reproduced the linear magnification factors from the outstanding model.

We present the results in Figure 12 assuming either parametric models or non-parametric models provided us with the true magnification and shear maps. The results in that figure show that the gravitational lensing models seem capable of predicting the linear magnification factors $\mu^{1/2}S^{1/2}$ to a value of 20 and 10 assuming that parametric and non-parametric models, respectively, represented the truth. Above these values, the median linear magnification factor no longer strongly correlate with the linear magnification factors in individual models.

If we assume that the parametric lensing models are plausible representations of the actual lensing model (as the tests of Meneghetti et al. 2017 suggest), this recommends that we linear magnification factors to a maximum of 20. For values above 20, it suggests we continue to suppose that the actual linear magnification is 20.

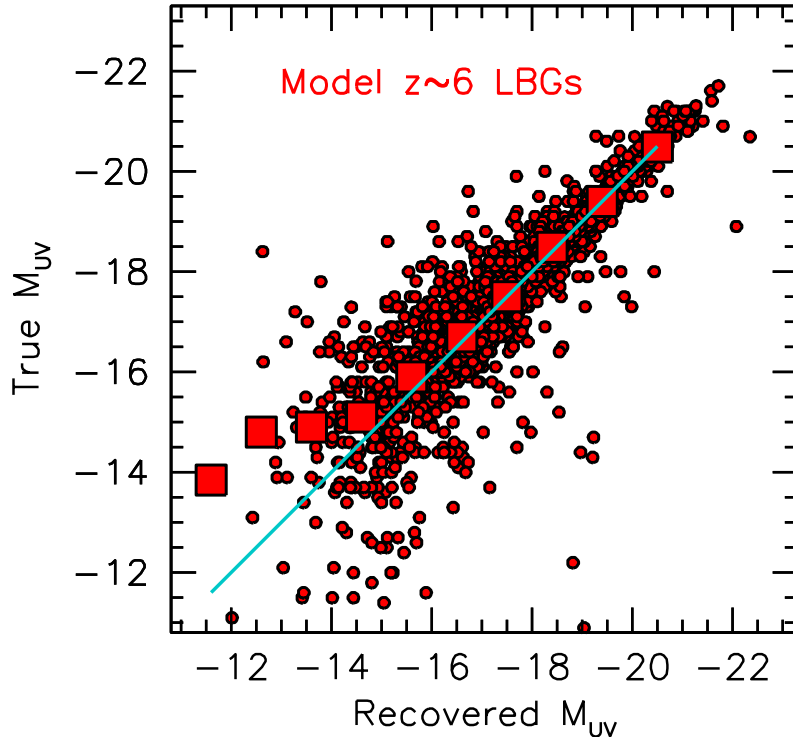


FIG. 13.— “True” UV luminosity vs. the UV luminosity estimated from the median parametric model for sources in a large forward-modeling simulation. The red circles show the original model UV luminosities plotted against the recovered UV luminosities from the median magnification maps. The red squares show the median “true” UV luminosity per magnitude bin of recovered UV luminosity. Importantly, the recovered median UV luminosity is never significantly fainter than -15 mag, for sources in the -14.5 mag, -13.5 mag, and -12.5 mag bins.

B. EXPECTED TRUE UV LUMINOSITIES VS. MODEL UV LUMINOSITIES

An important question regards the extent to which the inferred luminosities of sources behind the HFF clusters actually track their true luminosities. Addressing this question is not simple and requires significant testing through simulation and recovery experiments. Previous work included both model-to-model comparisons (Prieuwe et al. 2017; Bouwens et al. 2017b) and end-to-end tests (Meneghetti et al. 2017). These studies have demonstrated that lensing models appear to be reasonably predictive to a magnification of 30 in the median, but with 0.4-0.5 dex scatter (see e.g. Figure 3 from Bouwens et al. 2017b). Despite their utility, none of these tests were framed in terms of the UV luminosity in particular.

The purpose of this appendix is to look at the extent to which sources identified as having a given UV luminosity actually have that UV luminosity in the median. Framing the tests in terms of luminosity (instead of magnification) is valuable since sources from many different magnification and apparent magnitude bins contribute to a given bin in UV luminosity and the total volume within various bins of UV luminosity varies quite dramatically.

To determine how well the inferred UV luminosities actually track the true UV luminosities, we use the forward-modeling methodology described in Bouwens et al. (2017b). We use the v4.1 CATS magnification models to create mock catalogs over each of the first four HFF clusters, with each source being assigned coordinates and an apparent magnitude. Absolute magnitudes are then derived for sources in these catalogs based on the median magnification from the latest parametric lensing models.

Both the UV luminosities recovered and the true UV luminosities are presented in Figure 13. Also shown with the red squares are how well the luminosities of sources driven from the median magnification map predict the “true” model luminosities. Interestingly, the luminosities of sources inferred from the median magnification map track the actual model luminosities brightward of -15 mag, but fail to do so faintward of -15 mag. This suggests that it may be challenging to quantify with great confidence the properties or luminosity function of sources fainter than -15 mag.

C. SIZE MEASUREMENTS FOR THE FAINTEST $Z \sim 4$ GALAXIES IN THE HUDF

The sizes we infer for many lensed sources in our samples are much smaller than might be expected based on an extrapolation of the size-luminosity relation measured from field studies. While some trend might have been expected based on surface brightness selection effects at the low luminosity end of our samples, the fixed surface density of $z = 6-8$ galaxies vs. shear factor (Bouwens et al. 2017a) and high surface density of $z = 6-8$ galaxies even in high magnification regions suggests (§4.4) that our selections are not more incomplete to lower luminosity sources than high-luminosity sources. This suggests, as we highlighted in our discussions (§4.2-4.4), that lower-luminosity star-forming galaxies might therefore be genuinely small in terms of the observed UV light, especially when compared with extrapolated size-luminosity relations from Shibuya et al. (2015), for example.

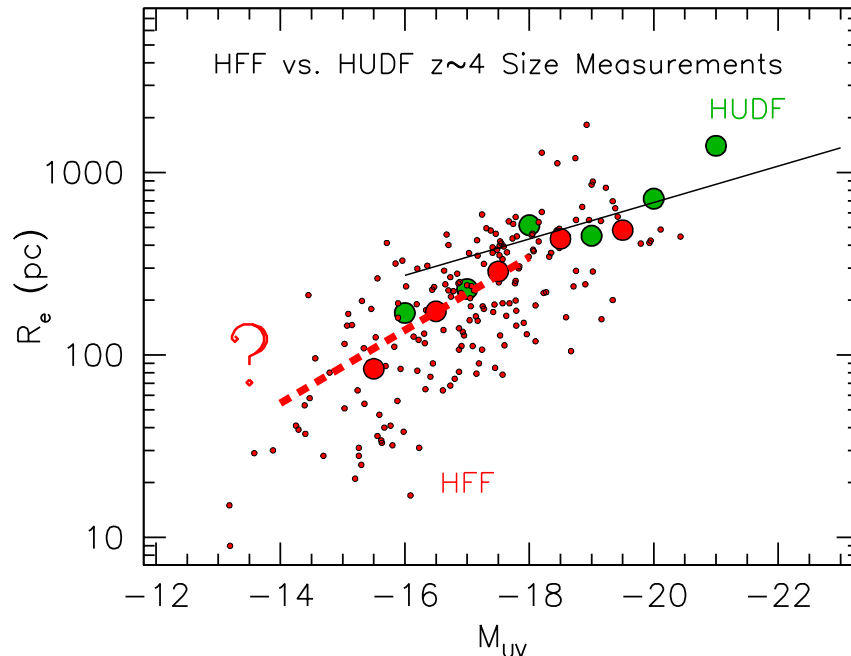


FIG. 14.— A comparison of the median sizes in specific UV luminosity bins measured from $z \sim 4$ galaxies in the HUDF (green circle) with the median sizes in specific UV luminosity bins measured from the $z \sim 4$ sample identified over the MACS0717 and MACS1149 HUDF clusters. The small red points show the size measurements for individual sources behind the HFF clusters. The black line shows the Shibuya et al. (2015) size-luminosity relation at $z \sim 4$. The red dashed line shows one possible size-luminosity relation that is both consistent with both our HUDF and HFF constraints and shows a steep luminosity dependence (where $r \propto L^{0.5}$). Encouragingly, while the size-luminosity relation at $z \sim 4$ can only be mapped to moderately low luminosities in the HUDF, the median size measurements derived from the HUDF agree with our HFF measurements at the faint end of our $z \sim 4$ selections. Not only does this support the reliability of the size measurements made based on our HFF samples are probably reliable, but it suggests that the size-luminosity relation may be steeper at the lowest luminosities.

It is challenging to test this at $z \geq 6$ with current field samples, as size measurements only probe down to -18 mag in our most sensitive blank field observations the HUDF. However, at lower redshifts, i.e., $z \sim 4$, one can systematically measure the size of galaxies to lower luminosities, i.e., -16 mag, where one might expect to see discrepancies between the extrapolated size-luminosity relation from Shibuya et al. (2015) and sources in the HUDF.

To this end, we made use of GALFIT (Peng et al. 2002) to measure source sizes for $z \sim 4$ galaxies in HUDF. Segregating sources as a function of luminosity, we compute the median sizes as a function of luminosity. We present the median sizes in Figure 14 vs. UV luminosity. For comparison, also shown in this same figure are the sizes of individual sources from a $z \sim 4$ selection using the HFF clusters (Bouwens et al. 2017, in prep) following the same method as described in §4.1. The median size constraints from our $z \sim 4$ HFF selection are included with the red circles.

Encouragingly enough, the median size measurements we derive from our $z \sim 4$ HUDF sample are in generally good agreement with that obtained from our $z \sim 4$ HFF sample, over the full range of luminosities. This suggests that the median size measurements that we obtain from lensed sources in the HFF data appear to be generally reliable. It is also interesting that the median size measurements for the faintest sources in the HUDF begin to fall below the size-luminosity relation seen for the brightest galaxies. While this may occur due to incompleteness in our selection of star-forming sources at $z \sim 4$ from the HUDF, it could also be providing us with evidence for a similar break in the size-luminosity relation in our $z \sim 4$ samples.

D. SIZE MEASUREMENTS FOR OTHER SOURCES IN OUR HFF SAMPLES

For future comparison studies, we also present in Table 4 our inferred size and luminosity measurements for the full set of 307 $z = 6-8$ sources utilized in this study, as well as spatial coordinates, total magnification factors, and linear magnification factors along the major shear axis.

TABLE 4
 PROPERTIES OF THE PRESENT COMPILATION $z = 6-8$ SOURCES OVER THE FIRST FOUR HFF CLUSTERS^a

ID	R.A.	Decl	M_{UV}	μ	μ_{1D}	r_e (pc)
A2744I-4205324088	00:14:20.54	-30:24:08.9	$-14.6^{+0.6}_{-0.6}$	$21.5^{+15.3}_{-8.8}$	$6.2^{+1.9}_{-2.5}$	17^{+28}_{-13}
A2744I-4222023578	00:14:22.21	-30:23:57.9	$-15.6^{+0.7}_{-1.2}$	$50.1^{+41.4}_{-33.6}$	$8.5^{+4.4}_{-3.8}$	31^{+32}_{-13}
A2744I-4212723104	00:14:21.28	-30:23:10.5	$-16.0^{+0.1}_{-0.1}$	$6.4^{+0.5}_{-0.8}$	$5.7^{+0.4}_{-1.2}$	32^{+24}_{-17}
A2744Y-4204124034	00:14:20.41	-30:24:03.5	$-14.0^{+1.2}_{-1.6}$	$75.0^{+151.2}_{-58.0}$	$15.1^{+24.0}_{-9.5}$	14^{+29}_{-9}
M0416I-6055105026	04:16:05.52	-24:05:02.7	$-14.6^{+1.4}_{-0.4}$	$18.0^{+47.0}_{-6.1}$	$16.3^{+35.8}_{-6.1}$	40^{+26}_{-27}
M0416I-6090604399	04:16:09.06	-24:04:40.0	$-15.3^{+0.3}_{-0.5}$	$11.6^{+3.4}_{-4.6}$	$7.3^{+2.4}_{-3.4}$	32^{+38}_{-13}
M0416I-6095704260	04:16:09.57	-24:04:26.1	$-15.0^{+0.3}_{-0.2}$	$12.5^{+3.3}_{-2.5}$	$8.0^{+2.5}_{-2.0}$	28^{+19}_{-12}
M0416I-6120203507	04:16:12.02	-24:03:50.8	$-13.6^{+1.2}_{-1.4}$	$62.7^{+121.6}_{-45.6}$	$57.6^{+91.5}_{-42.7}$	18^{+53}_{-11}
M0416I-6118103480	04:16:11.81	-24:03:48.1	$-15.0^{+1.3}_{-1.0}$	$33.6^{+81.6}_{-19.9}$	$24.5^{+85.1}_{-15.2}$	16^{+29}_{-13}

^a Table 4 is published in its entirety in the electronic edition of the Astrophysical Journal. A portion is shown here for guidance regarding its form and content.